Mechanisms of Physical-Biological-Biogeochemical Interaction at the Oceanic Mesoscale

Dennis J. McGillicuddy Jr.

Department of Applied Ocean Physics and Engineering, Woods Hole Oceanographic Institution, Woods Hole, Massachusetts 02543; email: dmcgillicuddy@whoi.edu

Keywords

eddies, eddy pumping, advection, eddy-wind interaction, eddy-driven stratification, plankton diversity

Abstract

Mesoscale phenomena are ubiquitous and highly energetic features of ocean circulation. Their influence on biological and biogeochemical processes varies widely, stemming not only from advective transport but also from the generation of variations in the environment that affect biological and chemical rates. The ephemeral nature of mesoscale features in the ocean makes it difficult to elucidate the attendant mechanisms of physical-biological-biogeochemical interaction, necessitating the use of multidisciplinary approaches involving in situ observations, remote sensing, and modeling. All three aspects are woven through this review in an attempt to synthesize current understanding of the topic, with particular emphasis on novel developments in recent years.

1. INTRODUCTION

Interconnection among the physics, biology, and biogeochemistry of the sea stems from three basic sources. First, the rates of biological and chemical reactions depend on environmental parameters such as temperature, salinity, and nutrient concentrations. Second, hydrodynamic transport continually redistributes dissolved and suspended constituents in the water column. Third, constituents of interest can have directed motion through the water as a result of buoyancy (sinking or floating) and behavior (swimming) in the case of motile organisms. Each of these three aspects supports a variety of mechanisms that create biological and biogeochemical variability at a wide range of temporal and spatial scales. For example, the difference in deepwater nutrient concentrations between the North Atlantic and North Pacific basins has been attributed to the joint effects of the global overturning circulation and remineralization of sinking particulate material (Broecker & Peng 1982).

A particularly strong manifestation of physical-biological-biogeochemical interactions takes place at the oceanic mesoscale. The currents, fronts, and eddies that make up this class of phenomena occur on spatial scales of tens to hundreds of kilometers and are in many ways dynamically analogous to atmospheric weather. Mesoscale motions are typically produced by instability processes that result in flow features that are in approximate geostrophic balance in the horizontal and in hydrostatic balance in the vertical; they are characterized by small Rossby and Froude numbers as well as small aspect ratios. Of course, mesoscale flows occur within a continuum of scales. They are bounded on one end of the spectrum by the large scale, which sets the mean gradients from which eddies are generated. At the other end of the spectrum, they are bounded by the submesoscale, where motions are also significantly influenced by rotation and stratification, but ageostrophic effects are important in the balance of forces. Although the dynamics of mesoscale eddies and fronts are closely related, I focus here mostly on the former.

Mesoscale eddies play a fundamental role in ocean circulation and dynamics (reviewed in McWilliams 2008). Targeted studies of their biological impacts date back at least as far as the late 1970s and early 1980s (**Supplemental Table 1**; follow the **Supplemental Materials link** from the Annual Reviews home page at **http://www.annualreviews.org**). Pingree et al. (1979) pioneered interdisciplinary investigations of eddies in shelf seas. Some of the first synoptic maps of phytoplankton, primary production, and seston in the open ocean were collected during the POLYMODE program, providing evidence of eddy-driven variations in all of these quantities (Radchenko 1983, Roukhiyainen & Yunev 1983). Near the same time, advances in remote sensing yielded the first satellite-based estimates of chlorophyll (CHL), indicating a variance spectrum consistent with geostrophic turbulence (Gower et al. 1980). Detailed interdisciplinary process studies of Gulf Stream rings began in that same era, focusing on eddy-induced variability and regional impacts (Ring Group 1981). These developments led to advancements in the conceptual basis for mesoscale physical-biological interactions (Legendre & Demers 1984, Mackas et al. 1985, Woods 1988).

Interest in the large-scale integrated impacts of eddies on ocean biogeochemistry was stimulated by the apparent discrepancy between estimates of new production and nutrient supply through vertical mixing (Jenkins & Goldman 1985, Shulenberger & Reid 1981). Specifically, mesoscale processes were hypothesized to be responsible for the "missing" nutrients in the subtropical gyre (Jenkins 1988a). Debate on the eddy-driven nutrient source in the subtropics has continued through the present time, whereas more recent studies suggest that eddies may constitute a net sink of nutrients in the subpolar gyre and in coastal upwelling regions. Several new research topics have also emerged, including the role of eddies in plankton patchiness, plankton community structure and biodiversity, and influences on higher trophic levels.

This review is an attempt to synthesize our understanding of mesoscale physical-biological-biogeochemical interactions, with particular emphasis on progress over the last 15 years. One new development during this time period was the analysis of both data and models in eddy-centric coordinates to illuminate the underlying dynamics; this approach is described in Section 2. This framework is used in Section 3 as a basis to survey the mechanisms by which eddies can influence upper-ocean CHL distributions. Eddy impacts on mean properties and fluxes are reviewed in Section 4, followed by descriptions of three relatively new and growing areas of inquiry: eddy-driven biological Reynolds stresses (Section 5), controls on community composition and diversity (Section 6), and mesoscale niche utilization by higher trophic levels (Section 7). Section 8 provides concluding remarks. This work builds on earlier reviews by Angel & Fasham (1983), Flierl & McGillicuddy (2002), Lewis (2002), Lévy (2008), Oschlies (2008), Klein & Lapeyre (2009), and Williams & Follows (2011; see chap. 9). Mahadevan (2016) reviews submesoscale physical-biological interactions elsewhere in this volume.

2. A NEW WINDOW INTO PHYSICAL-BIOLOGICAL INTERACTIONS AT THE MESOSCALE: ANALYSIS IN EDDY-CENTRIC COORDINATES

Recent progress in automated methods for identifying and tracking mesoscale eddies with satellite altimetry has facilitated construction of a global atlas of eddy trajectories, amplitudes, and sizes (Chelton et al. 2011b) (**Figure 1**). Use of the derived eddy-centric coordinates to merge
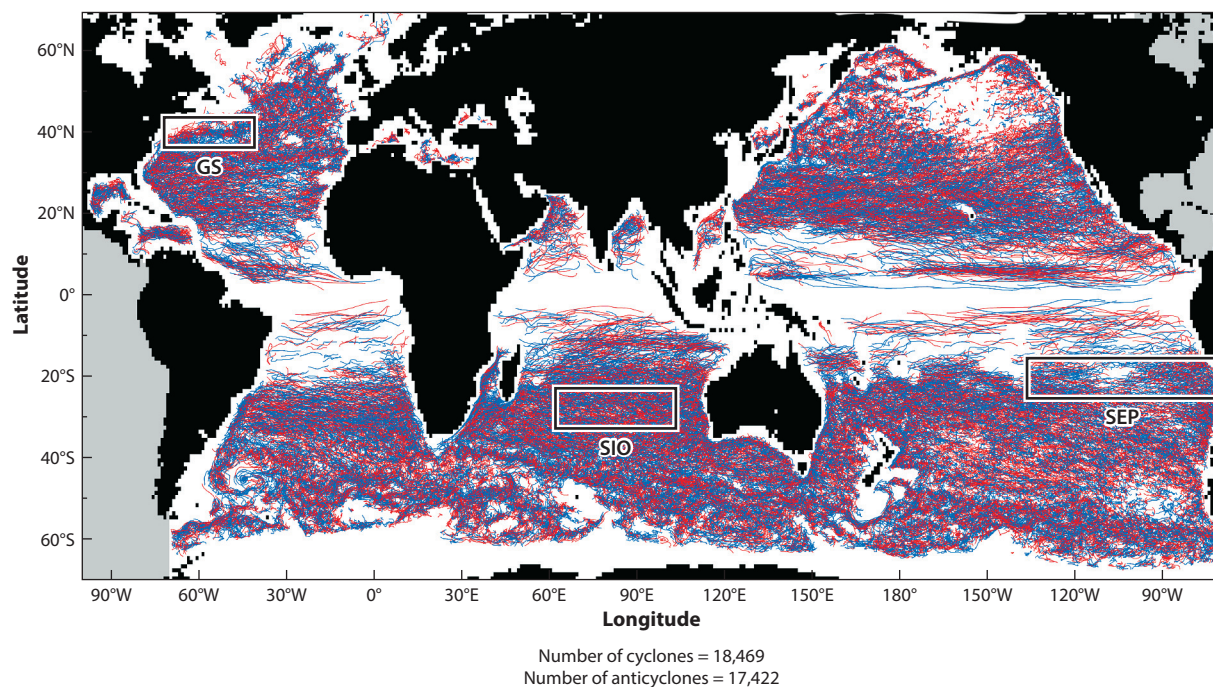

Number of cyclones = 18,469
Number of anticyclones = 17,422

Figure 1

Tracks of long-lived (lifetimes of ≥16 weeks) mesoscale eddies identified by an automated eddy tracking procedure applied to altimetric data for the period 1992–2008. Blue tracks represent cyclones; red tracks represent anticyclones. Three regional subdomains are indicated: the Gulf Stream region (GS), the South Indian Ocean (SIO), and the Southeast Pacific (SEP). Figure adapted from Chelton et al. (2011b) with permission.

altimetric sea surface height (SSH) data with other remotely sensed properties such as satellite ocean color (CHL), sea surface temperature (SST), and ocean vector winds is now providing unprecedented opportunities for investigation of the physical and biological dynamics of mesoscale phenomena. Construction of eddy-centric composites of many (in some cases, thousands) of synoptic realizations of satellite data has allowed mean eddy-driven signals to emerge. These coherent eddy-driven structures in surface properties vary regionally, reflecting a variety of mechanisms by which mesoscale dynamics can influence upper-ocean CHL distributions (Gaube et al. 2014).
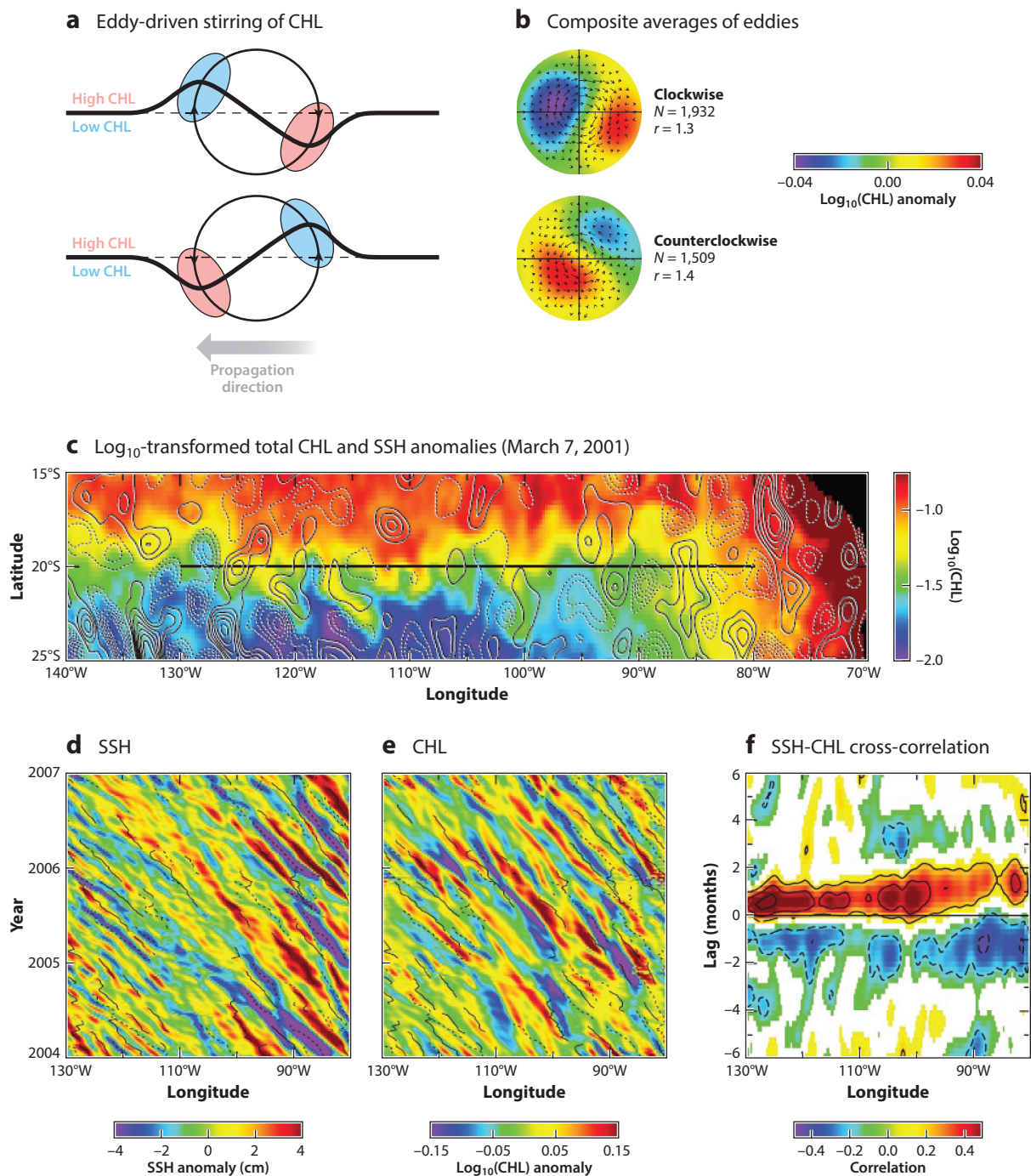
A key initial finding from the eddy-centric analysis of satellite-derived SSH was the degree of nonlinearity of mid-ocean eddies. Whereas earlier assessments of the westward-propagating signal in SSH based on a single altimeter were attributed to linear Rossby wave dynamics (Chelton & Schlax 1996), higher-resolution data products from multiple satellite missions merged together (Pascual et al. 2006) yielded a different picture. Chelton et al. (2007) computed a nonlinearity parameter from the ratio of the altimetrically inferred geostrophic swirl velocity (u) to the propagation speed (c) of each eddy feature and found that the vast majority of eddies were nonlinear ($u/c > 1$). This finding has key implications for interpretation of the associated biological signal: Nonlinear eddies trap fluid and their associated planktonic ecosystems inside them, whereas linearly propagating wavelike disturbances do not.

Initial investigations of the relationships between satellite-based SSH and CHL revealed coherence in large-scale westward-propagating signals that were attributed to linear Rossby waves (Cipollini et al. 2001, Uz et al. 2001), analogous to Chelton & Schlax's (1996) assessment of westward-propagating signals in SSH alone. A variety of mechanisms were proposed to explain the observed coherence in SSH and CHL, including (*a*) lateral advection of the mean CHL gradient, (*b*) uplift of the deep CHL maximum into the surface layer, (*c*) enhancement of phytoplankton biomass stimulated by upwelling of nutrients, and (*d*) accumulation of material in convergence zones within the planetary wave field (Charria et al. 2003, Dandonneau et al. 2003, Killworth et al. 2004). These early studies focused on large-scale signals characteristic of Rossby waves by processing the satellite measurements with scale-selective filters, and in some cases (Killworth et al. 2004) by utilizing only a single altimeter and thus a lower-resolution data set.

Using the new global database of eddy trajectories, Chelton et al. (2011a) overlaid eddy tracks on the westward-propagating signals previously attributed to Rossby waves in the filtered SSH and ocean color data (**Figure 2d,e**). The coincidence of those features strongly suggests that eddies are

Figure 2

(*a*) Schematic diagram of eddy-driven stirring of chlorophyll (CHL) for eddies rotating clockwise (*top*) and counterclockwise (*bottom*) and propagating westward in regions where the CHL gradient is northward. Otherwise smooth contours of CHL (*dashed lines*) are distorted by the rotational velocity field within the eddies, as shown by the solid lines. Advection of CHL within the large-scale background CHL gradient results in the positive and negative CHL anomalies shown by the red and blue regions, respectively. (*b*) Composite averages for clockwise (*top*) and counterclockwise (*bottom*) eddies in the Southeast Pacific (SEP) region indicated in **Figure 1**. The outer perimeter of each circle corresponds to twice the eddy radius scale. The vectors in each panel are the gradient of the composite average sea surface height (SSH), which is proportional to the geostrophic velocity. The number of eddy realizations (*N*) in the composite average and the magnitude of the ratio (*r*) of the primary pole in the leading (*left*) half of each composite to the secondary pole in the trailing (*right*) half are labeled. (*c*) An example map from the SEP region for March 7, 2001, showing $\log_{10}$(CHL) in color with contours of positive and negative anomalies of SSH (*solid* and *dotted lines*, respectively) at intervals of 2 cm, excluding the zero contour. The horizontal line indicates the section along which the time-longitude plots in panels *d* and *e* are presented. (*d*) SSH with eddy tracks within ±2° of 20°S overlaid (*dashed* and *solid lines* for clockwise- and counterclockwise-rotating eddies, respectively). (*e*) $\log_{10}$(CHL) with the same eddy tracks overlaid. (*f*) Lagged cross-correlation between $\log_{10}$(CHL) at time t and SSH at time $t +$ lag, calculated over the full ten-year data record; the white areas correspond to correlations smaller than the estimated 95% significance level. Positive lags correspond to $\log_{10}$(CHL) leading SSH, and the contour interval is 0.2, with the zero contour omitted for clarity. Figure adapted from Chelton et al. (2011a) with permission.

a Eddy-driven stirring of CHL

b Composite averages of eddies

High CHL
Low CHL

High CHL
Low CHL

Propagation direction

Clockwise
$N = 1,932$
$r = 1.3$

Counterclockwise
$N = 1,509$
$r = 1.4$

−0.04　　0.00　　0.04
$Log_{10}(CHL)$ anomaly

c Log_{10}-transformed total CHL and SSH anomalies (March 7, 2001)

Latitude

Longitude

$Log_{10}(CHL)$

−1.0

−1.5

−2.0

d SSH

e CHL

f SSH-CHL cross-correlation

Year

Longitude

Longitude

Lag (months)

Longitude

−4　−2　0　2　4
SSH anomaly (cm)

−0.15　−0.05　0.05　0.15
$Log_{10}(CHL)$ anomaly

−0.4　−0.2　0.0　0.2　0.4
Correlation

driving the observed CHL variations. How might eddies be aliased into a larger-scale Rossby wave signal? The westward propagation of both types of features stems from the latitudinal dependence of the effects of Earth's rotation, causing them to translate at approximately the same speed. In essence, a patchwork of westward-propagating eddies has a zonal wavenumber-frequency spectrum that is qualitatively similar to that expected for linear Rossby waves, which explains why eddies can pass through the filters intended to eliminate them in earlier studies (McGillicuddy 2011).

These findings require reassessment of the underlying mechanisms used to explain satellite observations of variability in SSH and upper-ocean CHL. Although the same four basic processes of biomass modulation mentioned above remain valid, their expression takes different dynamical forms at various scales, ranging from the mesoscale down to the submesoscale (Abraham 1998, Lévy et al. 2001, Siegel et al. 2008). In the next section I survey the various mechanisms that influence upper-ocean CHL, focusing on the mesoscale.

3. SURVEY OF MECHANISMS BY WHICH EDDIES AFFECT UPPER-OCEAN CHLOROPHYLL DISTRIBUTIONS

The following subsections describe various mechanisms of mesoscale physical-biological interaction, as manifested in their impacts on near-surface CHL. Some relate to transport (e.g., stirring and trapping), whereas others modulate biological rates in association with variations in nutrient and/or light availability (e.g., eddy pumping, eddy-wind interaction, and eddy impacts on mixed-layer depth). Each process thus produces a distinct local perturbation to the upper-ocean ecosystems, the integrated impacts of which are explored in Sections 4–7.

3.1. Eddy Stirring

Turbulent advection by mesoscale and submesoscale flows has long been recognized as a source of phytoplankton patchiness in the ocean (for a review, see Martin 2003). Idealized models of two-dimensional geophysical flows reveal the cascade of variance from large to small scales via stirring of populations (Abraham 1998), although in some instances biological dynamics can dominate (Srokosz et al. 2003). Direct observational evidence of mesoscale stirring has been derived from remotely sensed synoptic snapshots of surface geostrophic velocity (from altimetry) and CHL (Lehahn et al. 2007). Advanced algorithms for diagnosing various phytoplankton functional types have facilitated investigation of stirring effects on fluid dynamical niches (d'Ovidio et al. 2010).

From an eddy-centric perspective, rotational flow tends to perturb the local CHL distribution via azimuthal advection. Consider, for example, a clockwise-rotating eddy (Northern Hemisphere anticyclone) in a northward CHL gradient, shown schematically in the top part of **Figure 2***a*. The western (leading) edge of the eddy contains a negative CHL anomaly in the northwest quadrant, and the eastern (trailing) edge contains a positive CHL anomaly in the southeast quadrant. In the same background field, a counterclockwise-rotating eddy (Northern Hemisphere cyclone) will result in a positive anomaly in the southwest quadrant and a negative anomaly in the northeast quadrant (bottom part of **Figure 2***a*). The orientation of the dipole in CHL anomaly is a function of the rotational sense of the eddy (clockwise versus counterclockwise) as well as the propagation direction relative to the ambient CHL field.

Eddy stirring has been investigated in detail in the eastern subtropical South Pacific (Chelton et al. 2011a). Eddies in this region (labeled SEP in **Figure 1**) have a smaller mean amplitude (mean SSH anomaly = 3.2 cm) than the global average for the same latitude band (mean SSH anomaly = 6.2 cm), although their radial scale is approximately the same (110 km). As such, these eddies tend to be less nonlinear than the global average, with $u/c > 1$ for 87% of them. A complex relationship exists between SSH and CHL (**Figure 2***c*), with eddy-driven perturbations most

pronounced in the areas with the strongest CHL gradients. A strong mean gradient in CHL is also present in this region, oriented meridionally in the western part and zonally in the eastern part in proximity to the coast. Removing the large-scale gradients and mean seasonal cycle allows the eddy signals to emerge more clearly. Westward copropagation of SSH and CHL is readily apparent, and individual eddy trajectories delineate the streaks in the anomaly fields (**Figure 2d,e**). Compositing the data into eddy-centric coordinates, oriented relative to the large-scale mean gradient, yields dipole patterns characteristic of eddy stirring (**Figure 2b**). Although the dipole structures are qualitatively similar to the theoretical prediction (**Figure 2a**), there is a subtle difference: The magnitudes of the leading poles are higher in amplitude than the trailing poles. This asymmetry is apparently a result of the trailing edge of the eddy interacting with an ambient CHL field that has recently been under the influence of the leading edge of the eddy (Chelton et al. 2011a). Similar dipole patterns emerged from an eddy-centric analysis of eddy features in the Sargasso Sea (Siegel et al. 2011).

3.2. Eddy Trapping

Nonlinear eddies tend to trap the fluid contained in their interiors (d'Ovidio et al. 2013, Flierl 1981, Provenzale 1999). The composition of the trapped fluid depends on the process of eddy formation as well as on the local gradients in physical, chemical, and biological properties. These properties can be maintained over long time periods, depending on eddy evolution and exchange with the surrounding water masses. Gulf Stream rings provide a classic example (Wiebe & Joyce 1992) (**Figure 3a**). Cyclonic meanders pinch off cold-core rings that trap nutrient-rich, high-CHL slope water from the landward side of the Gulf Stream, whereas anticyclonic meanders pinch off warm-core rings that trap oligotrophic low-CHL water from the Sargasso Sea. A contrasting example comes from the Leeuwin Current (**Figure 3b**), which can spawn anticyclonic eddies with enhanced CHL derived from the coastal region (Moore et al. 2007). Trapped fluid is not unique to rings and boundary currents, and it is a common characteristic of nonlinear eddies in the open ocean (e.g., Menkes et al. 2002).

The trapping mechanism is evident in eddy-centric composites from the Gulf Stream region (Gaube et al. 2014). Cyclones from this region (labeled GS in **Figure 1**) contain positive CHL anomalies in their interiors, and anticyclones contain negative CHL anomalies (**Figure 4a**, sub-panels *i* and *ii*). In both cases, the anomalies appear as a monopole structure, in contrast to the dipole structure produced by eddy stirring (**Figure 2b**). More importantly, these CHL anomalies are present at the initial time of eddy detection (**Figure 4a**, subpanels *iii* and *iv*), suggesting that they originated from the process of eddy formation. Note that the region over which this analysis was performed is large enough to include not only Gulf Stream rings but also mid-ocean eddies; there is no distinction between them in the eddy-centric composites. In some regimes, such as the Agulhas retroflection, fluid trapped in rings can propagate well into the ocean interior, providing significant lateral fluxes of physical, chemical, and biological properties (Lehahn et al. 2011).

3.3. Eddy Pumping

Eddy pumping can be conceptualized by considering a density surface with a mean depth coin-cident with the base of the euphotic zone. This surface is perturbed vertically by the formation, evolution, and destruction of mesoscale features. Three types of features are schematized in **Figure 5**. Cyclones and anticyclones dome and depress the seasonal and main pycnoclines, respectively. Mode-water eddies are composed of a lens-shaped disturbance that raises the seasonal pycnocline and lowers the main pycnocline. During eddy formation and intensification
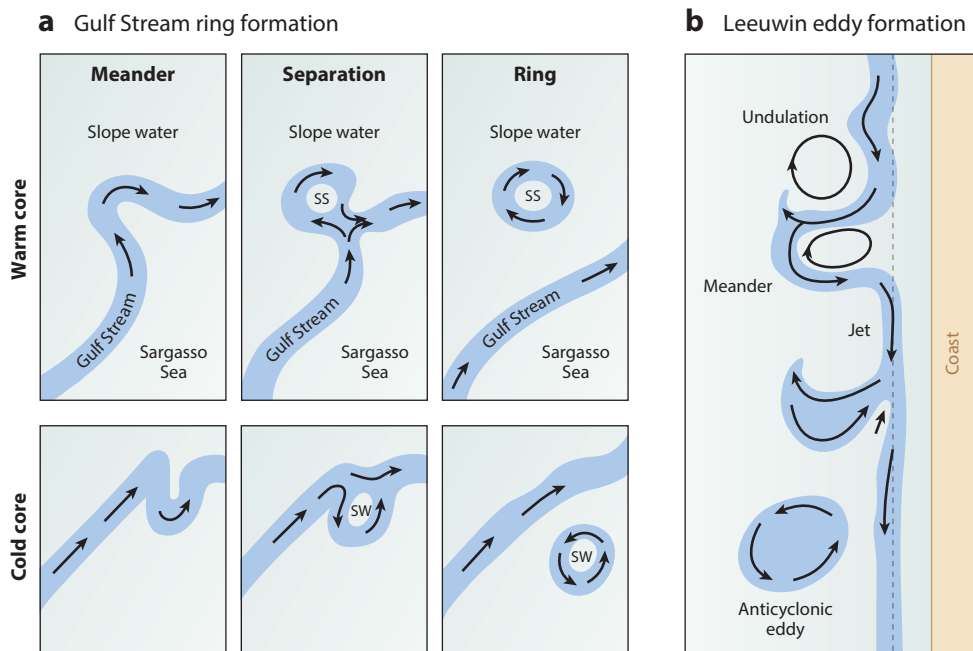
a Gulf Stream ring formation

b Leeuwin eddy formation

Figure 3

Processes of (*a*) Gulf Stream ring formation and (*b*) anticyclone generation in the Leeuwin Current. Abbreviations: SS, Sargasso Sea water in warm-core rings; SW, slope water in cold-core rings. Panel *a* adapted with permission from Warm Core Rings Exec. Comm. (1982) (*top*) and Knauss (1978) (*bottom*); panel *b* adapted with permission from Moore et al. (2007) and Pearce & Griffiths (1991).

(**Figure 5a**), shoaling density surfaces in cyclones and mode-water eddies lift nutrients into the euphotic zone, where they are rapidly utilized by the biota. Deepening of the isopycnals in anticyclones pushes nutrient-depleted water out of the well-illuminated surface layers. The asymmetric light field thus rectifies vertical displacements of both directions into a net upward transport of nutrients. Two aspects of this process favor complete utilization of the upwelled nutrients. First, the timescale for biological uptake is fast (on the order of days) with respect to the physical supply mechanism (eddy lifetimes on the order of months). Second, because the nutrient enhancement takes place in the eddy's interior, the circulation tends to isolate it from the surrounding waters, which allows biomass to accumulate until the upwelled nutrients are exhausted.

Evidence for the eddy pumping mechanism is present in the eddy-centric anomalies from the Gulf Stream region (labeled GS in **Figure 1**). To begin with, the positive CHL anomaly monopoles in cyclones (**Figure 4a**, subpanel *ii*) and negative CHL anomaly monopoles in anticyclones (**Figure 4a**, subpanel *i*) are consistent with expectations based on the conceptual model for eddy pumping, although the monopole structures of these polarities are ambiguous with respect to eddy trapping and pumping (Gaube et al. 2014). As stated above (Section 3.2), the presence of these anomalies at the time of first detection is consistent with trapping. However, the signature of eddy pumping is manifested by a subtle trend that barely exceeds the associated uncertainties: As Gulf Stream cyclones intensify in the first 12 weeks of their lifetimes (**Figure 4a**, subpanel *iii*), CHL anomalies also increase (**Figure 4a**, subpanel *iv*). By contrast, the negative CHL anomaly in anticyclones is more stable over time during the same interval.
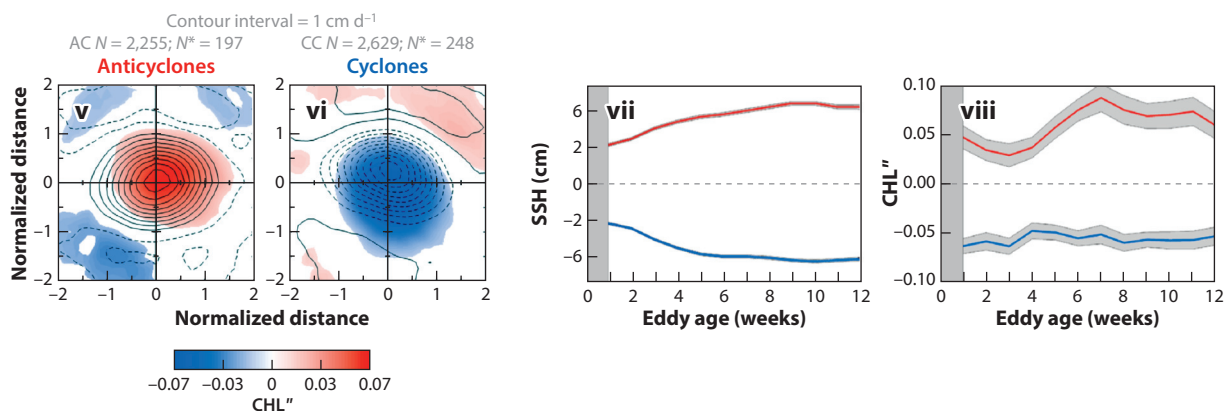
a Gulf Stream
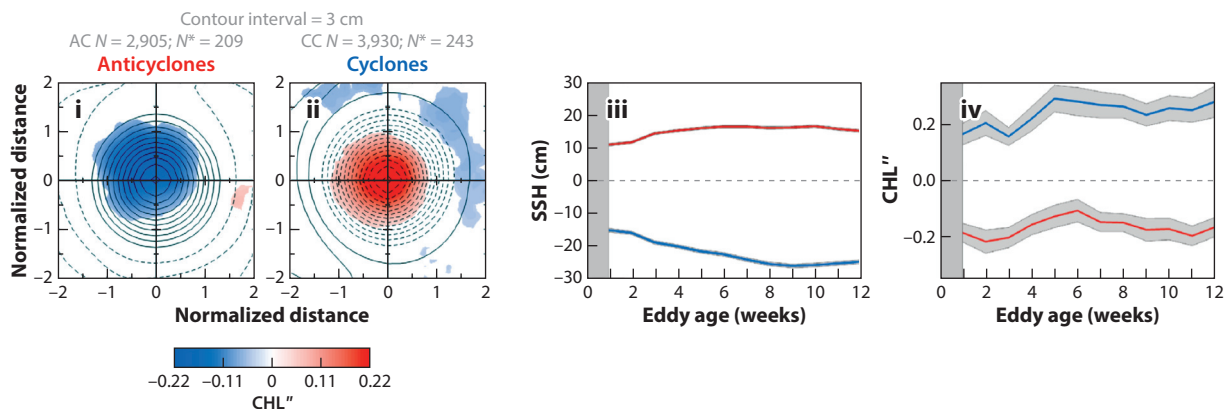
b South Indian Ocean

Figure 4

(*Left*) Composite averages of eddy-centric chlorophyll (CHL) anomaly in (*a*) the Gulf Stream region (year round) (subpanels *i* and *ii*) and (*b*) the South Indian Ocean (May–October) (subpanels *v* and *vi*). The locations of the two domains are shown in **Figure 1** (regions labeled GS and SIO, respectively). The contours in subpanels *i* and *ii* represent the sea surface height (SSH) anomaly, and those in panels *v* and *vi* represent eddy-induced Ekman pumping. Regions of the composites that do not exceed the 95% confidence interval of the mean are masked with white. The *x* and *y* coordinates of the composite averages are normalized by the eddy radius. Each composite average panel indicates both the number of eddy realizations (*N*) used to construct the composite and the effective degrees of freedom (*N**) used to compute the 95% confidence interval. (*Right*) Time series of eddy amplitude (subpanels *iii* and *vii*) and CHL anomaly (subpanels *iv* and *viii*) for cyclones (*blue*) and anticyclones (*red*). The beginnings of the time series are shaded to indicate that both eddy amplitude and CHL anomaly are observed only after the eddy is first detected by the automated eddy tracking procedure, defined here as week 1. Figure adapted from Gaube et al. (2014) with permission.

It is important to note that the eddy-centric analysis based on sea level cannot distinguish between mode-water eddies and regular anticyclones. Because steric height in mode-water eddies is dominated by downward displacement of the main pycnocline, they appear as positive anomalies in sea level, indistinguishable from regular anticyclones in terms of both SSH and their rotational velocities (McGillicuddy et al. 2007, Sweeney et al. 2003). As such, CHL anomalies generated by eddy stirring are expected to be the same in mode-water eddies as they are in regular anticyclones. By contrast, the expected response in terms of eddy pumping is confounding:
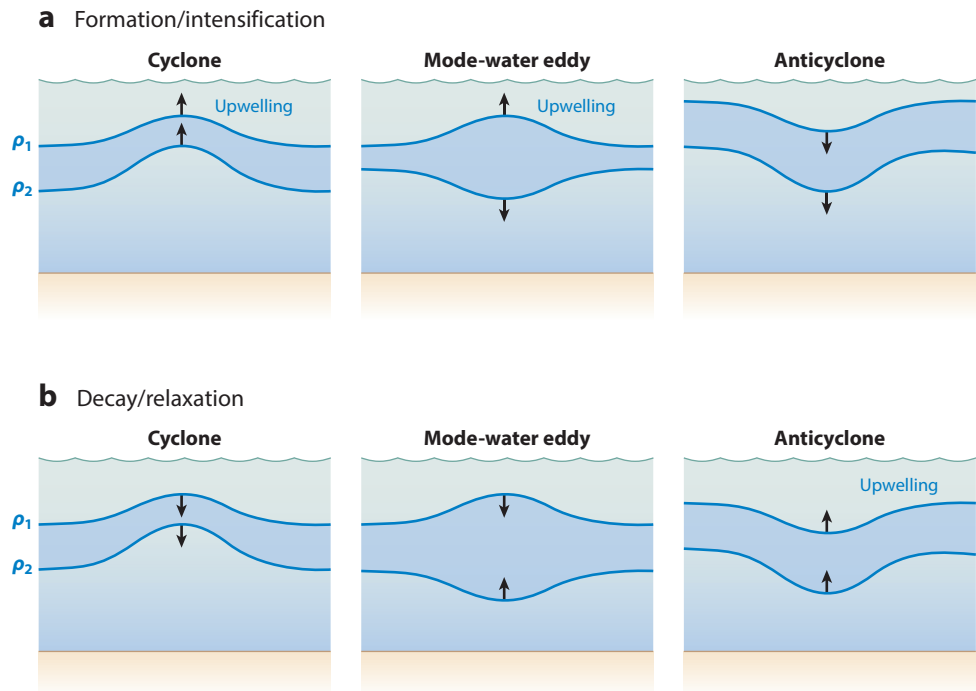
a Formation/intensification

b Decay/relaxation

Figure 5

Isopycnal displacements associated with three types of eddies in the process of (*a*) formation/intensification and (*b*) decay. Two density surfaces are depicted in each case: one in the seasonal thermocline (ρ_1) and one in the main thermocline (ρ_2). Figure adapted from Flierl & McGillicuddy (2002) with permission.

positive for intensifying mode-water eddies and negative for intensifying regular anticyclones. As for trapping, the CHL signature would depend on the ambient gradients and on whether the mechanism of formation was subduction from a remote source (Ebbesmeyer & Lindstrom 1986) or local generation through eddy-wind interaction (McGillicuddy 2015).

The eddy-induced vertical flux depends not only on the structure of the isopycnal displacements, but also on the sense in which they are being perturbed by eddy dynamics (upwelling versus downwelling). The latter characteristic is determined by the eddy's developmental stage as well as eddy-eddy interactions during its lifetime. During the process of eddy decay (**Figure 5b**), the sense of the vertical motions is opposite to that during formation/intensification: Relaxation of the density perturbations associated with eddy decay results in upper-ocean downwelling in cyclonic features and mode-water eddies while causing upwelling within anticyclones. An excellent example of the latter is provided by frictional spin-down of warm-core rings. A model by Franks et al. (1986) demonstrated how phytoplankton biomass enhancement could result from the nutrient input caused by the approximately 1 m d^{-1} vertical velocities at the ring center. Uptake rates of nitrate and silicic acid observed in the same ring were sufficient to utilize the upward flux of nutrients (Nelson et al. 1989).

3.4. Eddy-Wind Interaction

It was recognized long ago that the superposition of a wind-driven Ekman flow on a mesoscale velocity field gives rise to ageostrophic circulations involving significant vertical transports (Niiler
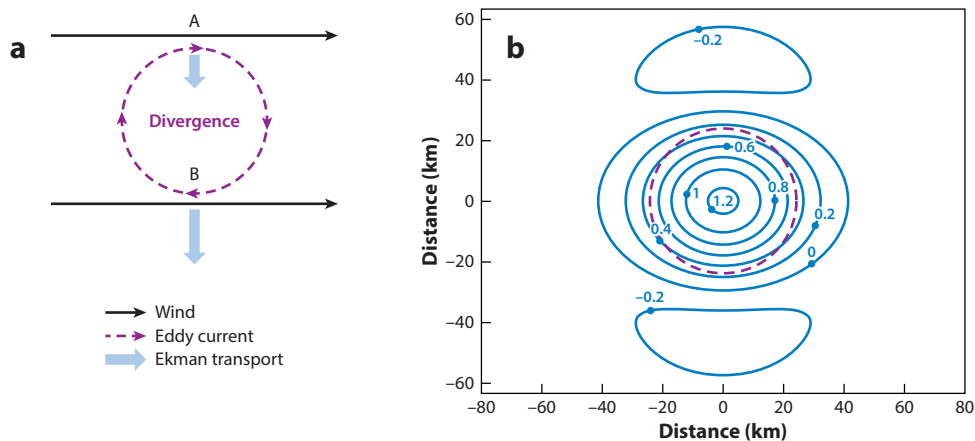
Figure 6

(*a*) Illustration of how a uniform wind applied to an anticyclonic eddy can lead to a divergence and upwelling in the eddy interior. The surface current reduces the stress where the wind is in the same direction as the current (point A) and increases it where the wind and current oppose each other (point B). The difference in the magnitude of the associated Ekman transport creates a divergence at the eddy center regardless of the direction of the wind. (*b*) Vertical velocity field at the base of the Ekman layer for an idealized circular eddy subject to a 15 m s^{-1} wind. The contour intervals are 0.2 m d^{-1}, with positive values denoting upwelling. The purple dashed line corresponds to the radius at which the maximum azimuthal velocity occurs. Figure adapted from Martin & Richards (2001) with permission.

1969, Stern 1965). Submesoscale patches of vertical velocity result from the generalized Ekman divergence, which includes vortex-stretching terms associated with advection of the interior vorticity by the boundary-layer velocity. For a uniform wind stress applied to a radially symmetric eddy, this effect creates a dipole of upwelling and downwelling, the structure of which depends on the direction of the wind and the vorticity of the eddy (see figure 4.33 in Flierl & McGillicuddy 2002).

The presence of mesoscale variability in the ocean affects the wind stress via two different processes. First, there is a feedback from SST. Cooler ocean temperatures tend to stabilize the marine atmospheric boundary layer, decoupling it from winds aloft. Conversely, warmer ocean temperatures tend to destabilize the boundary layer, thereby decreasing vertical shear in the wind. The net effect is to increase surface wind speeds over warmer water and decrease them over colder water, leading to measurable differences in wind stress, its curl, and therefore Ekman pumping (Chelton et al. 2004). Second, there is a direct effect on the wind stress caused by eddy-driven surface currents. That is, higher stress occurs on the flank of the eddy where the wind opposes the surface current, and lower stress occurs on the flank of the eddy where the wind and the current are in the same direction (**Figure 6a**). The net result is Ekman suction (upwelling) in the interiors of anticyclones (Dewar & Flierl 1987, Martin & Richards 2001) (**Figure 6b**) and Ekman pumping (downwelling) in the interiors of cyclones (Gaube et al. 2013, McGillicuddy et al. 2007). In contrast to the prior two mechanisms of eddy-wind interaction, the vertical velocity field resulting from eddy-induced Ekman pumping is a monopole located at the eddy center that does not depend on the direction of the wind.

Gaube et al. (2015) assessed the relative magnitudes of these three processes and found that the SST effect is generally smaller than the other two. The magnitudes of the vertical velocities induced by vorticity advection tend to be larger than those arising from eddy-induced Ekman pumping. However, the integrated impact depends critically on the structure of the associated

vertical velocity fields. Specifically, the relative persistence of the monopole generated by the surface current stress effect overshadows the constantly fluctuating dipole created by vorticity advection (see figures 8 and 9 in Gaube et al. 2015).

In nutrient-limited conditions, eddy-induced Ekman pumping is thus expected to produce positive CHL anomalies in anticyclones (upwelling) and negative CHL anomalies in cyclones (downwelling). This is precisely the pattern observed in eddy-centric composites of CHL anomalies and eddy-induced Ekman pumping from the South Indian Ocean (**Figure 4b**, subpanels *v* and *vi*). Time series of CHL anomalies (**Figure 4b**, subpanels *vii* and *viii*) reveal that these anomalies are present at the time of eddy detection, suggesting that the eddy-trapping mechanism is also at work. Indeed, both satellite data and in situ process studies (Moore et al. 2007, Waite et al. 2007) have shown that high-CHL waters of coastal origin can be entrained into anticyclones of the Leeuwin Current (**Figure 3b**). However, the time series presented in **Figure 4b**, subpanels *vii* and *viii*, also show that the positive CHL anomalies in anticyclones are significantly higher in weeks 6–11 as compared with weeks 1–4, which is consistent with eddy-induced Ekman pumping. Martin & Richards (2001) cited this process as a potential contributor to nutrient flux in an anticyclone in the northeast Atlantic. Eddy-induced Ekman pumping has also been invoked as an explanation for an extraordinary bloom of diatoms deep in the euphotic zone of a mode-water eddy in the Sargasso Sea (McGillicuddy et al. 2007) as well as near-surface CHL variations in the South China Sea (Li et al. 2014). By contrast, Eden & Dietze (2009) found that eddy-induced Ekman pumping decreased overall productivity in a model of the North Atlantic—a result of the fact that this process accelerates eddy decay (Dewar & Flierl 1987), thereby decreasing eddy kinetic energy and the associated nutrient supply.

3.5. Impacts on Mixed-Layer Depth

The presence of geostrophic motions and their associated vorticity produce local variations in the effective Coriolis frequency, which can affect propagation characteristics of near-inertial waves (e.g., Kunze 1985). Regions of negative vorticity can focus and amplify such waves, thereby augmenting shear, which potentially leads to increased vertical mixing. Simulations by Klein & Hua (1988) illustrated the mesoscale heterogeneity in mixed-layer depth that can arise from this process in a quasi-geostrophic flow field forced by a uniform wind. This inertial Ekman pumping creates a broad spectrum of variations in mixed-layer depth, although an eddy-scale signal is prominent.

Mixed-layer depth is also modulated by the local changes in stratification driven by eddy-induced vertical isopycnal displacements. For example, in a cyclonic eddy, upward doming of the pycnocline increases stratification in the upper ocean, thereby shallowing the mixed-layer depth for a given amount of turbulent kinetic energy from the surface. Conversely, downward deflection of the pycnocline by an anticyclonic eddy tends to reduce upper-ocean stratification, thereby allowing the same amount of turbulent kinetic energy to create a deeper mixed layer. These direct impacts of the local stratification tend to be augmented by air-sea heat flux anomalies resulting from the associated perturbations in SST (Williams 1988). For example, consider a situation in which the mean SST is such that there is no net sensible heat transfer to or from the atmosphere. Cold SST anomalies in cyclones tend to draw heat into the ocean from the atmosphere, further increasing stratification in those features relative to the ambient waters. Similarly, warm SST anomalies in anticyclones tend to release heat from the ocean into the atmosphere, cooling the surface ocean and thereby enhancing convection. The tendency for anticyclonic eddies to have deeper mixed layers than cyclones has been noted in the Gulf Stream (Dewar 1986), the northeast Atlantic (Williams 1988), the North Pacific (Kouketsu et al. 2012), and the South Indian Ocean (Dufois et al. 2014, Gaube et al. 2013). In fact, Dufois et al. (2014) have offered deeper mixed
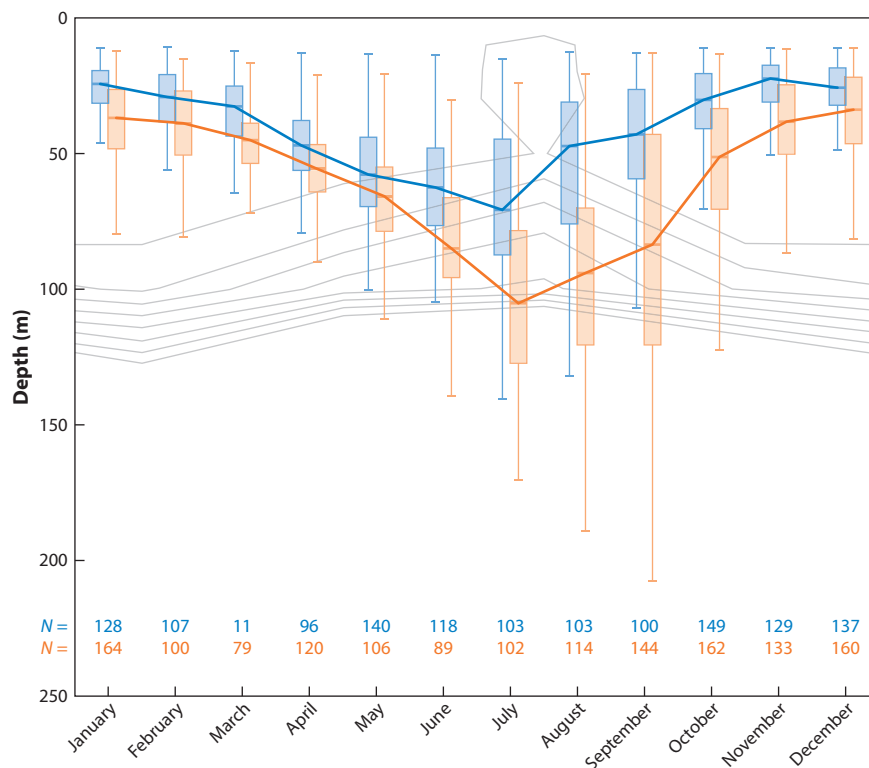
Figure 7

Climatological average mixed-layer depths in cyclonic (*blue*) and anticyclonic (*orange*) eddy interiors from Argo floats in the South Indian Ocean (region similar to the one labeled SIO in **Figure 1**). The number of floats (*N*) used for each month is also shown. The thin gray lines correspond to the NO_3 mean seasonal contours (from NOAA 2009) ranging from 0.3 to 1 mmol m^{-3}. For each time point, the rectangular box is delimited by the lower quartile (Q1) and upper quartile (Q3), and the median is represented inside the box by a straight line. Whiskers are drawn to the extreme values that are inside the fences lying at Q1 − [1.5 × (Q3 − Q1)] and Q3 + [1.5 × (Q3 − Q1)]. Bold lines join median values. Figure adapted from Dufois et al. (2014) with permission.

layers (**Figure 7**) as an alternative explanation for long-lived CHL anomalies in anticyclones of the South Indian Ocean (**Figure 4b**, subpanels *v–viii*). Differentiating between enhanced mixing and eddy-induced Ekman pumping is difficult in this case, as both mechanisms tend to produce CHL anomalies of the same sign in this nutrient-limited regime. In a light-limited regime, eddy-driven variations in mixed-layer depth would presumably produce CHL anomalies of the opposite sign: Shallower mixed layers in cyclones would lend themselves to higher CHL, and deeper mixed layers in anticyclones would lend themselves to lower CHL (**Table 1**).

3.6. Mechanisms of Chlorophyll Enhancement in the Peripheries of Anticyclonic Eddies

In contrast to the dipole and monopole anomalies of CHL described above, annular ring-shaped patterns have been observed around the peripheries of eddies, particularly anticyclones. Although

Table 1 Upper-ocean chlorophyll (CHL) anomalies expected from anomalies in mixed-layer depth (MLD) associated with cyclones and anticyclones in different regimes limited by nutrients and light

Eddy type	MLD anomaly	CHL anomaly	
		Nutrient limited	Light limited
Cyclone	−	−	+
Anticyclone	+	+	−

Note: This idealized summary does not represent mode-water eddies, which constitute a special case of anticyclones.

such patterns have yet to emerge in eddy-centric composites, synoptic snapshots have revealed these features in a variety of regimes, including the Southern Ocean (Kahru et al. 2007) (**Figure 8*a,b***), the Gulf of Alaska (Mizobata et al. 2002), and the Mozambique Channel (José et al. 2014). Qualitatively similar patterns have been produced in a variety of models (José et al. 2014, Lapeyre & Klein 2006, Lévy & Klein 2004, Lima et al. 2002, Mahadevan et al. 2008) (**Figure 8*c,d***). Two basic mechanisms have been invoked to explain these annular patterns: (*a*) lateral entrainment of streamers of high-CHL water from nearby coastal or frontal regions, and (*b*) local enhancement via either stratification in light-limited systems or nutrient supply via upwelling along the eddy periphery. The latter can arise in submesoscale patches of upwelling and downwelling associated with meandering of the circular front that delineates the outer edge of an eddy (McGillicuddy et al. 1995). Upwelling rates in such features can be as high as $10–100$ m d^{-1} as a result of eddy-wind, eddy-eddy, and/or eddy-front interactions (Mahadevan et al. 2008, Martin & Richards 2001, Yoshimori & Kishi 1994).

Upwelling rates that occur at the submesoscale can be much larger than those characteristic of the eddy scale itself. However, these intense vertical motions are also associated with swift horizontal currents characteristic of frontal regions. As such, a water parcel transported into the euphotic zone by a submesoscale upwelling cell can be rapidly advected into a submesoscale downwelling cell, where it can then be transported back out of the euphotic zone. The degree to which the upwelled nutrients are utilized by the biota depends on the relative timescales of the supply and uptake processes, which of course is a function of the dynamical regime and the local chemical and biological environment (for a review, see Williams & Follows 2003). Another key factor is the degree of reversibility along the upwelling and downwelling trajectory. Both vertical mixing and lateral dispersion can lend a degree of irreversibility to the process, making the nutrient content of the downwelled water less than that of the upwelled water, resulting in a net transport of nutrients (Martin & Richards 2001, Martin et al. 2001).

Figure 8

(*a,b*) A large anticyclonic eddy north of the mean position of the Southern Antarctic Circumpolar Current front (*black curve*) on January 28, 2004, showing chlorophyll (CHL; panel *a*) and sea surface temperature (SST; panel *b*). Ocean areas covered by clouds are shown in white. The white curves are edges determined on the CHL image but overlaid on both images. (*c,d*) Output from a numerical model highlighting an anticyclonic eddy. Negative relative vorticity in panel *c* [units of the Coriolis parameter $f = 2\Omega \sin(\text{latitude})$, where Ω is the Earth's rotation rate] is accompanied by a high phytoplankton concentration around the periphery of the vortex in panel *d*. Note that the sense of rotation is clockwise in panels *c* and *d* (Northern Hemisphere) and counterclockwise in panels *a* and *b* (Southern Hemisphere). Panels *a* and *b* adapted from Kahru et al. (2007) with permission; panels *c* and *d* adapted from Lévy & Klein (2004) with permission.

3.7. Global Perspective

Sections 3.1–3.6 illustrated the variety of mechanisms by which eddies can shape CHL distributions in the upper ocean. Examining the correlation between satellite measurements of SSH and CHL (**Figure 9**) provides a global perspective. Areas of positive correlation are indicative of positive CHL anomalies associated with anticyclonic eddies (positive SSH anomaly), and negative CHL anomalies are associated with cyclonic eddies (negative SSH anomaly). Conversely, regions of
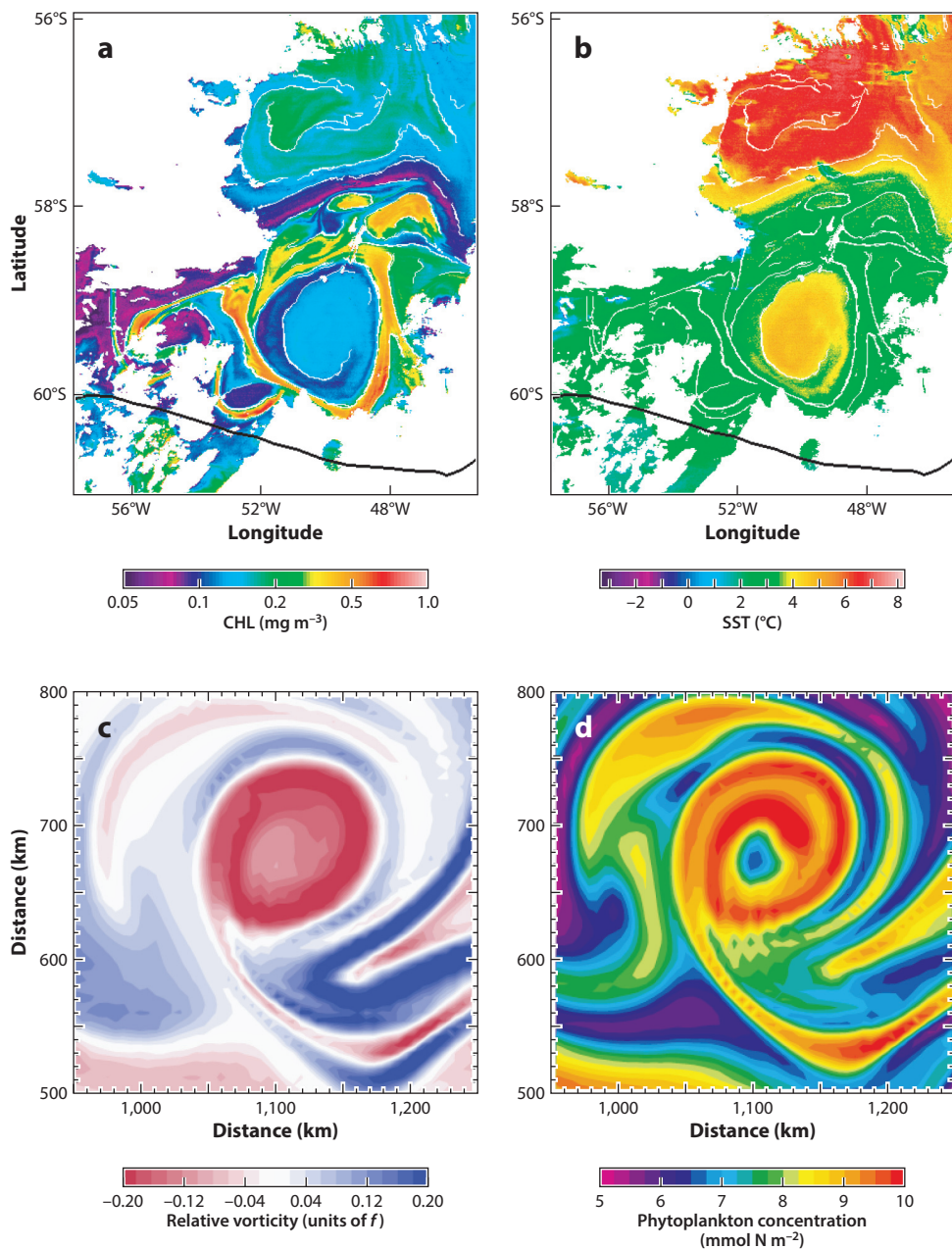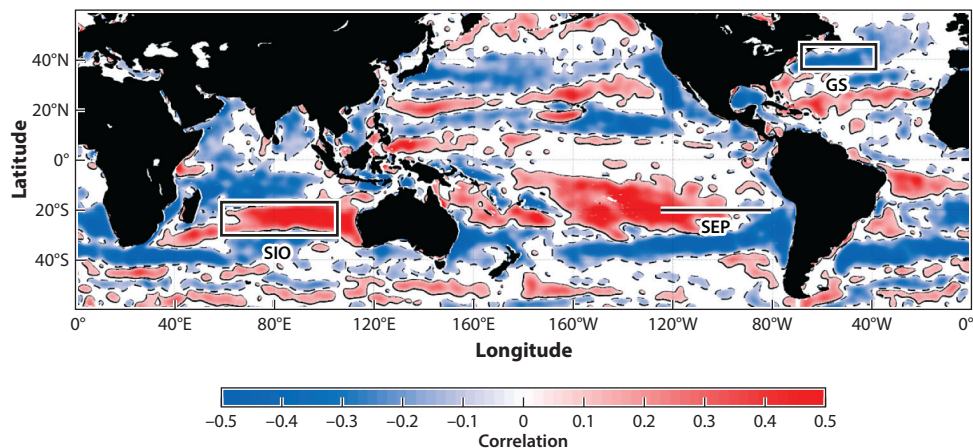
Figure 9

Map of the correlation between anomalies of sea level and chlorophyll. White areas correspond to correlations smaller than the estimated 95% significance level, and regions of significantly positive and negative cross-correlations are enclosed by solid and dashed contours, respectively. The regions indicated in **Figure 1** are also shown (SIO, South Indian Ocean; SEP, Southeast Pacific; GS, Gulf Stream). Figure adapted from Gaube et al. (2014) with permission.

negative correlation are indicative of positive CHL anomalies associated with cyclonic eddies and negative CHL anomalies associated with anticyclones. The coherent regional structure in this correlation strongly suggests systematic variations in the mechanisms of mesoscale physical-biological interactions in the global ocean (Gaube et al. 2014).

A prime example of negative correlation occurs in the Gulf Stream region. Eddy-centric analysis (**Figure 4a**, subpanels *i–iv*) suggests that both trapping (**Figure 3a**) and eddy pumping (**Figure 5**) are at work. Negative correlation is observed in other western boundary current systems and their midlatitude extensions, including the Kuroshio Current, the Agulhas Current, and the Brazil-Malvinas Confluence. Similarly, most eastern boundary current systems, such as the California Current, the Peru-Chile Current, and the Benguela Current, are characterized by negative correlation. Regions of negative correlation are also observed in the open ocean, such as areas to the northeast of Madagascar and to the east of the Hawaiian Islands in the North Pacific.

A prominent feature of positive correlation resides in the South Indian Ocean. Eddies in this region exhibit the signature of trapping, likely associated with high-CHL anticyclones and low-CHL cyclones spawned from the Leeuwin Current (**Figure 3b** and **Figure 4b**, subpanel *viii*). High CHL in anticyclones and low CHL in cyclones may be maintained by eddy-induced Ekman pumping (**Figure 4b**, subpanels *v* and *vi*) and/or eddy impacts on mixed-layer depth (**Figure 7**). These same mechanisms may be operating in other regions of positive correlation, such as the central South Pacific, subtropical North and South Atlantic, and around the Hawaiian Islands in the central North Pacific.

The SSH-CHL cross-correlation along the line in the southeast Pacific examined by Chelton et al. (2011b) (**Figure 9**) is consistent with **Figure 2f**, with negative values in the east and positive values in the west. However, the key to diagnosis of the eddy-stirring characteristic of the region (**Figure 2a,b**) lies in the time-lagged cross-correlation. The maximum positive correlation occurs when the SSH anomaly lags the CHL anomaly by approximately one month, whereas the maximum negative correlation occurs when the SSH anomaly leads the CHL anomaly by

approximately one month (**Figure 2f**). This is a result of the westward-propagating dipoles, in which positive and negative lobes of CHL anomalies are offset from the eddy center, where the extrema in SSH occur. Note that the negative correlation at −1 month lag tends to be weaker than the positive correlation at +1 month lag because the ambient CHL on the trailing edge of the eddy has been previously disturbed by advection from the leading edge (cf. **Figure 2b**).

In aggregate, these results highlight the utility of eddy-centric compositing to illuminate mechanisms of physical-biological interaction. However, limitations are also clear. For example, based on this information alone, a CHL response to upwelling/downwelling occurring during eddy intensification cannot be differentiated from the trapping of CHL during eddy formation in regions where the ambient CHL gradient favors enhanced (suppressed) CHL in the interiors of cyclonic (anticyclonic) eddies (e.g., the Gulf Stream). Likewise, a CHL response to eddy-induced Ekman pumping and/or eddy-driven perturbations to mixed-layer depth cannot be differentiated from the trapping of CHL in regions where the ambient CHL gradient favors enhanced (suppressed) CHL in the interiors of anticyclonic (cyclonic) eddies (e.g., the South Indian Ocean). The temporal evolution of the SSH and CHL signatures of eddies can help to address these ambiguities, but unequivocal diagnosis of the underlying mechanisms is not possible on the basis of satellite data alone. Moreover, the near-surface manifestation of mesoscale eddies in ocean color data may not always reveal the physical-biological dynamic in its entirety, insofar as large-amplitude biological responses can take place deep in the euphotic zone, where they are only partially detected by satellite (McGillicuddy et al. 2007). Thus, developing a more complete understanding of the role of mesoscale eddies in upper-ocean ecosystem dynamics and biogeochemical cycling will require detailed analysis of satellite observations together with subsurface in situ measurements and numerical simulations.

4. EDDY IMPACTS ON MEAN PROPERTIES AND FLUXES

Whereas the study of eddy-driven variability is guided by observations, quantification of their integrated impact on mean properties of the system and associated biogeochemical fluxes ultimately relies on models. A wide variety of approaches have been used to address this question, ranging from idealized process-oriented formulations to more realistic simulation-oriented configurations. These approaches are complementary in several ways, not the least of which is that the former provide conceptual frameworks for diagnosing more complex simulations. For example, Lee & Williams (2000) evaluated eddy-driven fluxes in a periodic channel forced with wind stresses and heat fluxes that mimic subtropical to subpolar environments. Adopting the formalism described by Gent et al. (1995), they derived eddy-induced advection and diffusion from the time-averaged and zonally averaged tracer equations. Their results showed that eddy-induced advection and diffusion of nutrients oppose each other in the upper ocean and reinforce each other in the deep ocean (**Figure 10a**). Wind-driven flows also play an important role in the near-surface layer (**Figure 10b**): Lateral Ekman fluxes into the subtropical gyre oppose the outward eddy-induced advection, and downwelling of nutrients driven by Ekman convergence counters upward eddy-induced advection (eddy pumping). Idealized models have also elegantly demonstrated that resolving mesoscale eddies may not be adequate for assessing the mean fluxes. Lévy et al. (2001) simulated frontal instability at resolutions of 10, 6, and 2 km and found that new production systematically increased with resolution. The productivity of the 2-km model was almost three times that of the 10-km model, clearly demonstrating the importance of submesoscale processes.

Truly eddy-resolving models have only recently been run on basin to global scales (Hecht & Hasumi 2008), and computational limitations generally preclude simulations much longer than 5–10 years for coupled physical-biological-biogeochemical applications. Such integrations are
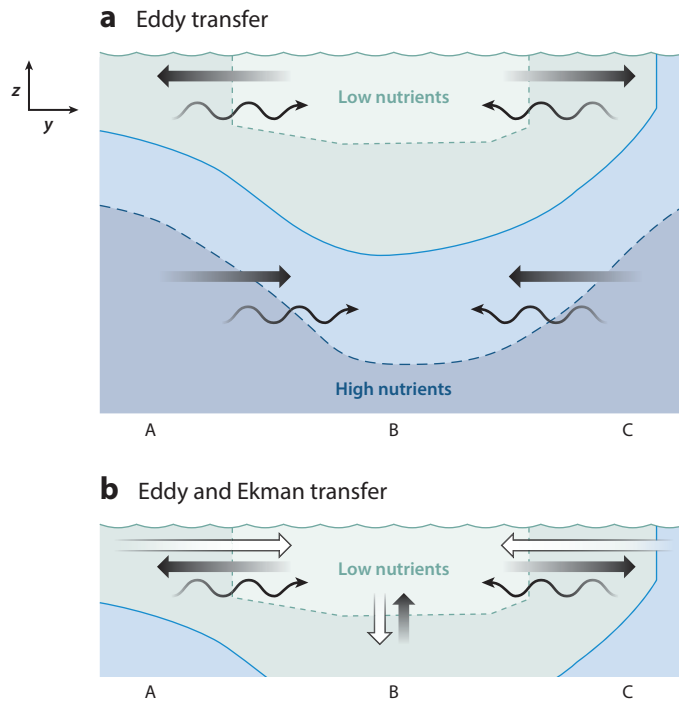
a Eddy transfer

b Eddy and Ekman transfer

Figure 10

Schematic of the eddy-induced transfer of nutrients. The region between points A and C may be viewed as passing through a subtropical gyre; the region between points A and B may be viewed as passing through the Southern Ocean. In panel *a*, the eddy-induced advection (*straight black arrows*) and diffusion (*wavy arrows*) oppose each other at the surface and reinforce each other at depth. In panel *b*, the Ekman advection (*white arrows*) is included. Figure adapted from Lee & Williams (2000) with permission.

typically long enough to provide several years of quasi-equilibrium solution for analysis subsequent to the transients associated with adjustment to initial conditions. However, these solutions can be far from true equilibrium, as illustrated in a recent study by Lévy et al. (2012b) comparing the results of 1/54°- and 1/9°-resolution models integrated for 50 years in an idealized double-gyre simulation reminiscent of the North Atlantic (**Figure 11**). After 50 years, the two models showed systematic regional differences in total production of $\pm 60\%$. A particularly salient feature of the higher-resolution model is the ~30% decrease in the productivity of the subtropical gyre, attributed to a long-term deepening of the nitracline in that region. In other words, mesoscale and submesoscale dynamics produce not only local fluctuations but also changes in the mean state of the system. This caveat must be kept in mind when interpreting the results from shorter-term integrations described below.

4.1. Subtropical Gyre

The role of eddies in supplying nutrients in the subtropical gyre has been debated for some time. Comparison of two hydrographic profiles sampled one month apart off Bermuda documented an apparently eddy-driven nutrient injection event that could account for 20–30% of the annual new production (Jenkins 1988b). High-resolution transects in the Pacific (Venrick 1990) and Atlantic (Strass 1992) revealed mesoscale variations in CHL consistent with eddy-induced upwelling.
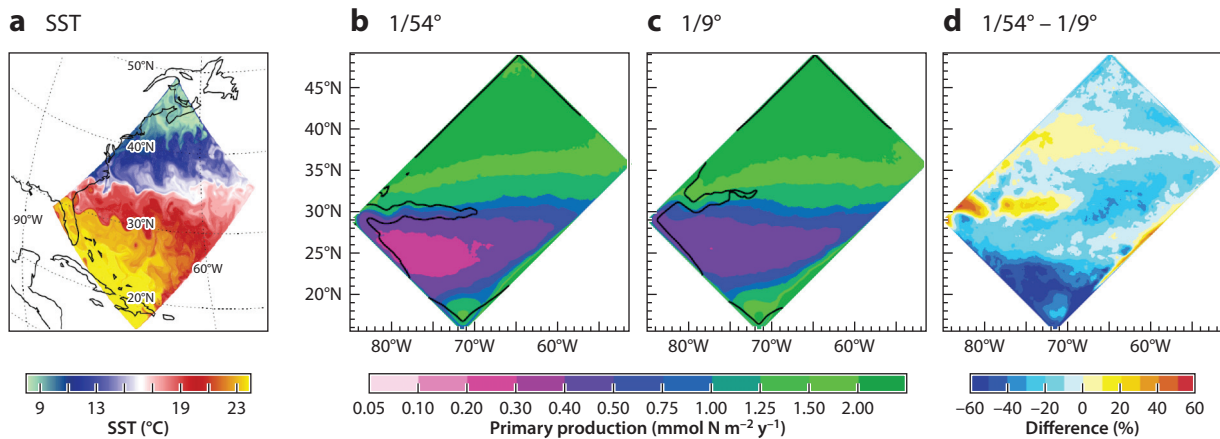
a SST

b 1/54°

c 1/9°

d 1/54° − 1/9°

SST (°C)

Primary production (mmol N m^{-2} y^{-1})

Difference (%)

Figure 11

(*a*) Sea surface temperature (SST) simulated in an idealized double-gyre system of the western North Atlantic. (*b–d*) Five-year average depth-integrated (0–120 m) primary production for 1/54°-resolution (panel *b*) and 1/9°-resolution (panel *c*) models after 50 years of integration, along with the difference between the two relative to the 1/9° model (panel *d*). Note that panel *a* uses a different map projection than panels *b–d* do. Panel *a* adapted from Lévy & Martin (2013) with permission; panels *b–d* adapted from Lévy et al. (2012b) with permission.

Surveys of a cyclone in the lee of Hawaii documented increased primary production in its interior, and extrapolation of that result suggested a 20% enhancement of global primary production by mid-ocean eddies (Falkowski et al. 1991). A variety of models have been brought to bear on this question, but the magnitude of the eddy-induced flux and its utilization is model dependent (Eden & Dietze 2009; Martin & Pondaven 2003; McGillicuddy & Robinson 1997; McGillicuddy et al. 1998, 2003; Oschlies 2002; Oschlies & Garçon 1998; Pasquero et al. 2005).

An example is provided in **Figure 12**, in which the horizontal and vertical nutrient fluxes in a one-tracer light-limited nutrient transport model have been decomposed into their time-mean and eddy-driven components. Although this decomposition is different from that used by Lee & Williams (2000) to distill **Figure 10**, some commonalities are evident in the results. In the subtropical gyre, mean vertical advection constitutes a sink of nitrate owing to the downwelling caused by Ekman convergence. Eddy-induced vertical advection is a source of nitrate, which is sufficient to overcome the mean downward transport such that the total vertical advection is a net source of nitrate. Note that Lee & Williams (2000) predicted the opposite, with Ekman downwelling overshadowing eddy pumping (**Figure 10***b*). In other aspects, the realistic simulation is more similar to the idealized model. Horizontal advection (**Figure 12**) is near zero over much of the subtropical gyre due to the low concentration of nitrate in the surface waters of this region. However, horizontal advection is a net source of nutrients along the northern edge of the gyre. This lateral flux of nitrate into the gyre arises mostly from the mean fields, roughly consistent with the Ekman flux of nitrate described by Williams & Follows (1998).

4.2. Subpolar Gyre

New production in the subpolar gyre is considerably higher than that in the subtropical gyre (**Figure 12**) owing to a combination of vigorous vertical mixing and mean upwelling from divergence of the wind-forced Ekman surface current. Interestingly, the time-varying component of vertical advection is negative over a large portion of this region, especially in areas where the

a New production

b Convection and vertical diffusion

c Total vertical advection

d Mean vertical advection

e Eddy vertical advection

f Total horizontal advection

g Mean horizontal advection

h Eddy horizontal advection

Nitrogen flux (mol m^{-2} y^{-1})

winter mixed-layer depth is greatest. In the southern part of the gyre, the magnitude of this sink is sufficient to overcome the mean upward vertical advection, causing the total vertical advection to be negative in that area. Horizontal advection is also important in this region. The large area of negative net lateral flux arises primarily from mean horizontal advection. Eddy-driven horizontal advection in this area varies on smaller scales but generally tends to reinforce the mean. This negative lateral flux results from the northeastward flow of the North Atlantic importing lower concentrations of nitrate into the subpolar gyre.

In contrast to the subtropical gyre, where eddy-driven fluxes constitute a net source of nutrients, it appears that the oceanic mesoscale has a significant impact on nutrient removal from the euphotic zone in the subpolar gyre. A similar feature is evident in the simulations of Oschlies (2002), suggesting that this result is not model dependent. Diagnosis of the solutions shown in **Figure 12** suggests that the downward nutrient flux results from mesoscale processes associated with restratification following deep convection (**Figure 13**). Indeed, mesoscale and submesoscale dynamics play a key role in the process of restratification (Mahadevan et al. 2012, Marshall 1997, Nurser & Zhang 2000). Lévy et al. (1998, 1999) described how mesoscale restratification increases productivity following convection by releasing phytoplankton from light limitation. The eddy-induced nutrient sink shown in **Figure 13** is the counterpart to that process deeper in the water column: The same mesoscale dynamics that restratify the near-surface region pump nutrients out of the euphotic zone. This removal takes place at a time when the ambient nutrients are in excess of limiting concentrations, so there is no immediate reduction of productivity. However, this process would tend to decrease productivity on seasonal to annual timescales, insofar as a portion of the nutrients brought into the euphotic zone by winter mixing are pumped back downward prior to utilization. On the other hand, Mahadevan et al. (2012) have suggested that the mixed-layer eddies involved in restratification could increase overall productivity.

4.3. Coastal Upwelling Systems

Upwelling regions along coastal margins support some of the most productive marine ecosystems on Earth. These systems also tend to have high eddy kinetic energy owing to the squirts, jets, filaments, and eddies that are formed when along-shore wind stress generates an Ekman divergence at the coast that leads to upwelling. In contrast to the oligotrophic waters of the subtropical open ocean, where eddy-induced nutrient fluxes can increase productivity, eddy-driven processes apparently decrease productivity in upwelling systems (Gruber et al. 2011; Lathuilière et al. 2010, 2011). Two mechanisms appear to be at work: lateral stirring and subduction.

First, stirring by mesoscale structures transports upwelling-derived biomass offshore, thereby reducing biomass in the upwelling zone itself. This process was noted by Rossi et al. (2008) in their analysis of finite-size Lyapunov exponents (FSLEs) and CHL distributions in the Benguela

←———

Figure 12

Five-year time-averaged (*a*) new production and (*b–h*) nutrient supply terms, integrated over the euphotic zone. Advective fluxes in the vertical (*middle row*) and horizontal (*bottom row*) have been separated into their mean and eddying components. All fields have been smoothed with a 24-point e-folding-scale Gaussian filter. Plus signs in panel *a* indicate the locations of several sites where the model was evaluated (BATS, Bermuda Atlantic Time-series Study; EUMELI, Eutrophic Mesotrophic Oligotrophic site; NABE, North Atlantic Bloom Experiment; OWSI, Ocean Weather Station India). Asterisks in panels *b–h* indicate the main features of the solutions described in the text, and the contours in panel *b* indicate maximum winter mixed-layer depths of 100, 300, and 500 m. Note that winter mixed layers inside the 500-m contour exceed that value by severalfold; additional contours are not shown for clarity of presentation. Figure adapted from McGillicuddy et al. (2003) with permission.
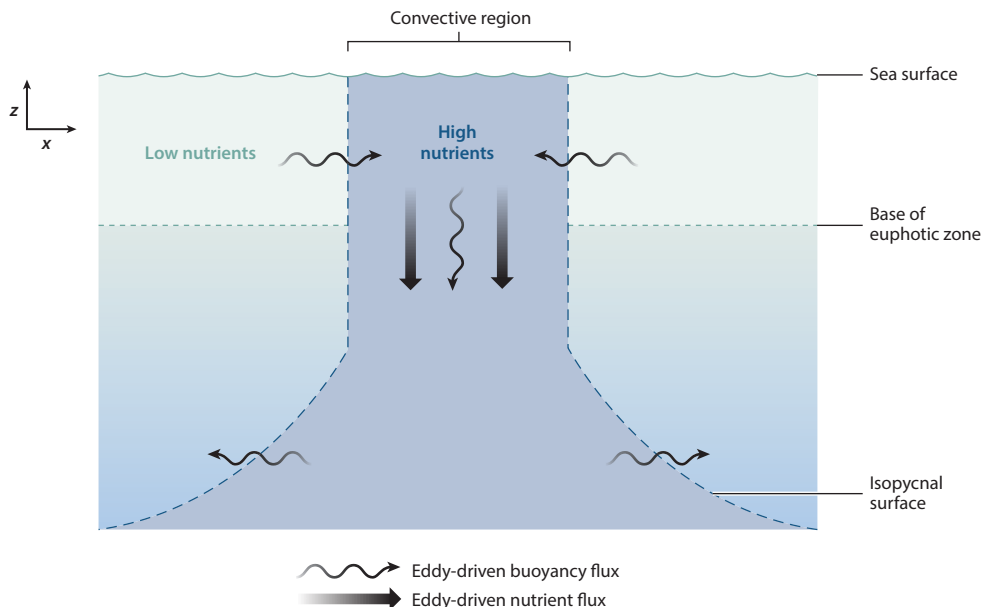
Figure 13

Schematic of the eddy-driven processes that tend to restratify an area of deep convection in the open ocean. An inward flux near the surface and outward flux at depth imply a downward eddy-driven transport that removes nutrients from the euphotic zone. Note that the convective area represents not an individual chimney but rather the larger region over which mesoscale and submesoscale convective events take place. Figure adapted from McGillicuddy et al. (2003) with permission.

and Canary upwelling systems. FSLEs provide a measure of lateral stirring and can be computed directly from satellite altimeter data. Rossi et al. (2008) found that CHL concentration is inversely correlated with FSLEs in these systems, such that the more vigorous stirring in the Benguela system was associated with CHL concentrations lower than those of the Canary system. The role of mesoscale processes in reducing phytoplankton biomass was quantified in a model of the Benguela system, indicating that eddy-driven transports are responsible for 30–50% of the offshore fluxes of biological tracers (Hernández-Carrasco et al. 2014).

The second mechanism involves offshore subduction of upwelled nutrients. Gruber et al. (2011) diagnosed the eddy-induced nitrogen fluxes from a high-resolution coupled physical-biological model of the California Current system (**Figure 14**). As expected, vertical eddy-induced fluxes are positive close to the coast, where mesoscale dynamics are intimately involved in the upwelling process. Lateral eddy fluxes transport nitrogen away from the coast in the surface layer in concert with downward eddy-induced transport offshore, and the net result is subduction into the ocean interior. These subducted nutrients occupy an intermediate layer that is distinct from the one that feeds the Ekman-driven upwelling cell, thus constituting a leak of nutrients that decreases the overall productivity of the system.

In addition to eddy-induced transports, special biogeochemical transformations take place within eddies in upwelling systems. For example, hot spots for fixed-nitrogen loss have been observed in association with anticyclonic eddies in the Peru oxygen minimum zone (Altabet et al. 2012, Bourbonnais et al. 2015, Stramma et al. 2013). However, observations of this process are currently so sparse that quantification of their integrated impact on nutrient budgets is not yet possible.
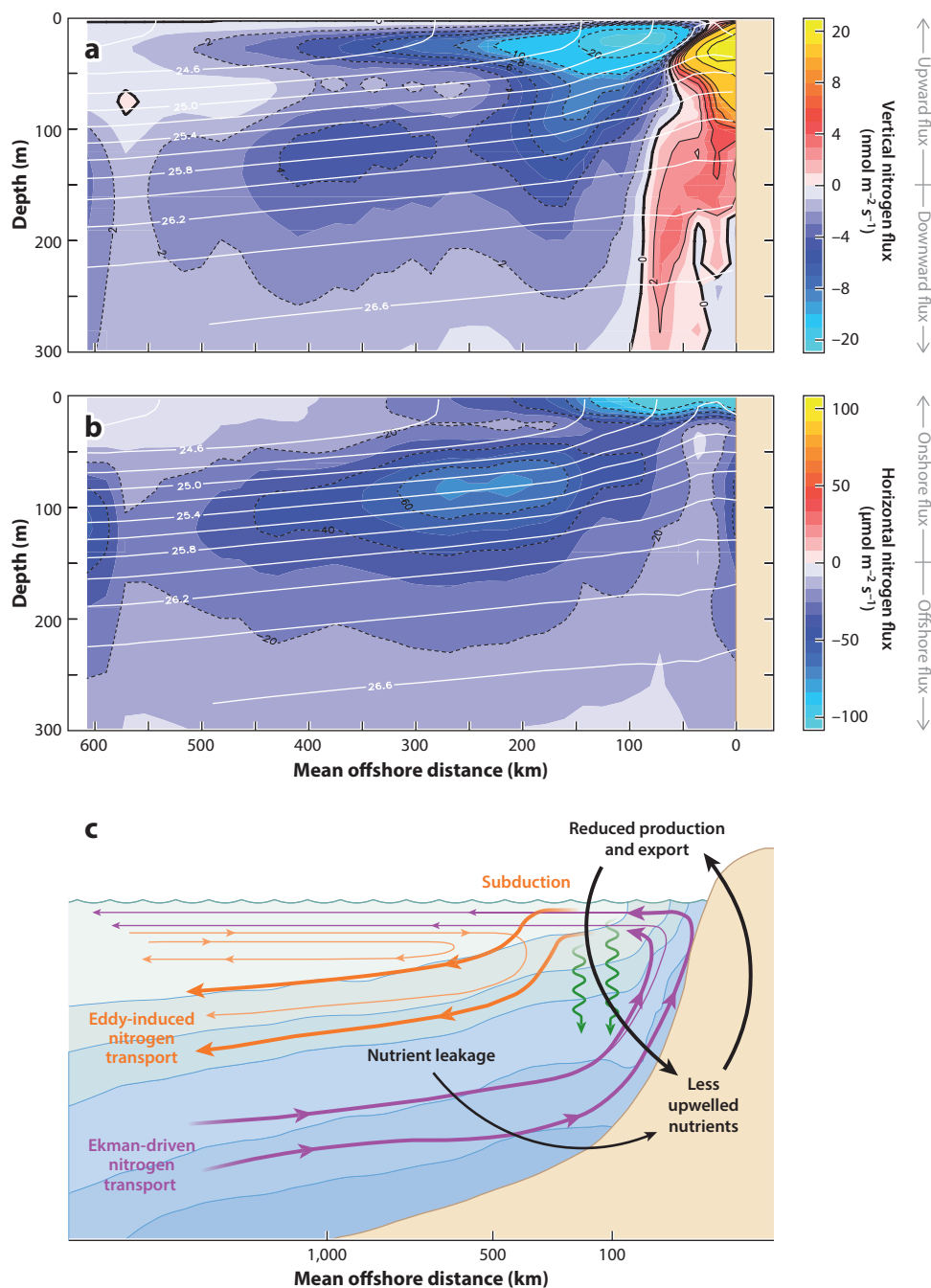
Figure 14

Cross-shore sections illustrating the role of eddies in inducing a lateral loss of total nitrogen from a model of the California Current system. (*a,b*) Vertical and horizontal fluxes of total nitrogen. White lines indicate potential density; black dashed lines indicate negative fluxes. (*c*) Conceptual diagram of the impact of mesoscale eddies on coastal circulation, nitrogen transport, and organic matter production and export. Thick lines indicate total nitrogen transport, and thin lines depict circulation pattern. Purple arrows indicate the Ekman-driven transports and circulations, orange arrows the eddy-driven transports, green arrows the vertical export of organic matter, and blue contour lines the potential density. Figure adapted from Gruber et al. (2011) with permission.

4.4. Other Regional Studies

Growing awareness of the diversity of eddy impacts on biological systems has led to increasing numbers of regional studies. For example, analysis of satellite-based observations of sea level and ocean color in the Weddell-Scotia Confluence in the Southern Ocean indicates that cyclonic eddies enhance biological production (Kahru et al. 2007). Both observations and models suggest that anticyclonic eddies enhance production in the northern Gulf of Alaska by virtue of the iron they transport from the coastal margin into the interior (Crawford et al. 2007, Xiu et al. 2011). A high-resolution model of the South China Sea suggests that cyclonic eddies are an important source of nutrients to the surface ocean in that region, triggering shifts in phytoplankton species composition toward diatoms, thereby increasing export flux and associated cycling of carbon (Xiu & Chai 2011). On the other hand, observations in the South China Sea have revealed enhanced export fluxes in anticyclones, attributed to submesoscale upwelling along eddy peripheries (Zhou et al. 2013; cf. Section 3.6). Using data from shipboard surveys, Prasanna Kumar et al. (2007) estimated that eddy pumping increases productivity in the Bay of Bengal by 50–100%. In a model of the Arabian Sea, Resplandy et al. (2011) found that multiple mesoscale processes contributed to regional nutrient budgets, namely (*a*) lateral advection from coastal upwelling zones into the interior via jets and filaments, (*b*) eddy pumping, and (*c*) eddy-driven restratification following monsoonally driven convective mixing. Such integrative analyses seeking to assess the net impact of eddies on various systems draw heavily on the growing amount of data provided by in situ process studies (**Supplemental Table 1**).

Supplemental Material

5. EDDY-DRIVEN BIOLOGICAL REYNOLDS STRESSES

Many biological processes relevant to plankton ecosystems are intrinsically nonlinear, and thus the average response of a population to a fluctuating environment can be quite different from the response of an average organism to average conditions. Three-dimensional coupled physical-biological models are typically formulated in terms of the mean field approximation, in which properties φ_i in a given grid cell are assumed to be adequately represented by their mean value $\overline{\varphi_i}$. The Reynolds decomposition expresses the full field as a sum of mean and fluctuating components, the latter of which average to zero: $\varphi_i = \overline{\varphi_i} + \varphi_i'$. Even though $\overline{\varphi_i'} = 0$, the average value of a nonlinear biological function f operating on the fluctuations $\overline{f(\varphi_i')}$ does not necessarily vanish. Moreover, the average product of two constituents $\overline{\varphi_i \varphi_j}$ includes contributions not only from the means $\overline{\varphi_i}\,\overline{\varphi_j}$ but also from the biological Reynolds stresses $\overline{\varphi_i' \varphi_j'}$. These effects have been examined in a variety of idealized frameworks, including theoretical (Goodman 2011, Goodman & Robinson 2008), one dimensional (Brentnall et al. 2003), and two dimensional (Wallhead et al. 2008), quantifying the limitations of the mean field approximation in such systems.

The net impact of fluctuations in biological properties has only recently been examined in three-dimensional simulations of mesoscale and submesoscale turbulence (e.g., Wallhead et al. 2013). Lévy & Martin (2013) diagnosed these terms from their 1/54°-resolution physical-biological model of the North Atlantic, making a distinction between eddy reactions and eddy transports of the type described in Section 3. Their findings illustrate that the eddy reaction terms play qualitatively different roles for different state variables (see figure 9 in Lévy & Martin 2013). For nitrate, the eddy reactions are generally small relative to the mean biogeochemical reactions, with the latter being balanced by a complex, latitudinally dependent combination of vertical mixing, mean advection, and eddy transport. By contrast, eddy reactions are among the largest terms in the phytoplankton equation, negative in sign and varying inversely with the mean reaction term. In other words, nonlinear interactions at the mesoscale and submesoscale reduce primary productivity. For

zooplankton, the eddy reactions vary with latitude: They are small south of 28°N, increase secondary productivity between 28°N and 40°N, and decrease secondary productivity north of 40°N. Although the details of these diagnoses may be model dependent, these findings clearly illustrate that eddy-driven fluctuations can be rectified by nonlinear biogeochemical transformations—and that the magnitudes of the eddy reactions are on the order of 5–15% of the means (see figure 7 in Lévy & Martin 2013). Whereas complete knowledge of a modeled system lends itself to relatively straightforward computation of biological Reynolds stresses, observational assessment is made more challenging by the lack of multiscale resolution of all relevant quantities. Initial attempts to quantify eddy-driven biological Reynolds stresses suggest more modest magnitudes than those derived from models (Martin et al. 2015).

6. INFLUENCES ON PHYTOPLANKTON COMMUNITY COMPOSITION AND DIVERSITY

Eddy-induced disturbances in the physical and chemical environment can bring about changes in the communities of primary producers. In fact, such biological responses may regulate the net impact on biogeochemical fluxes described above. For example, Goldman (1988) suggested the "spinning wheel" concept, in which the background state of oligotrophic systems is dominated by small phytoplankton growing primarily on nutrients that are recycled through the microbial loop. This state is episodically perturbed by the input of nutrients to the base of the euphotic zone, causing a shift in phytoplankton species composition from picoplankton toward much larger cells, such as diatoms. In such a scenario, these large cells would sink rapidly once the nutrient enhancement was depleted, thereby contributing a disproportionately large fraction of new versus total primary production. Laboratory culture experiments have confirmed that diatoms can grow rapidly enough to produce significant blooms even at the low light levels characteristic of the base of the euphotic zone (Goldman & McGillicuddy 2003). Indeed, evidence for mesoscale variations in diatom abundance has been observed in a variety of oceanographic environments, including the North Pacific (Brzezinski et al. 1998), Hawaiian lee eddies (Olaizola et al. 1993, Seki et al. 2001, Vaillancourt et al. 2003), the Hawaii Ocean Time-series site (Letelier et al. 2000), the Sargasso Sea (Krause et al. 2010, McGillicuddy et al. 2007), and the Bermuda Atlantic Time-series Study site (Krause et al. 2009, McNeil et al. 1999, Sweeney et al. 2003). Bibby & Moore (2011) found that the response of diatom populations to eddy-induced upwelling in the subtropical Atlantic and Pacific depends on the nitrate-to-silicate ratio of the upwelled water. In several cases, mesoscale diatom blooms have been linked directly to enhanced particle export (Allen et al. 2005, Benitez-Nelson et al. 2007, Bidigare et al. 2003).

Even more general relationships between the mesoscale environment and plankton community structure have emerged from both observations and models. For example, Rodriguez et al. (2001) identified a linear relationship between the size-abundance spectrum of phytoplankton and vertical velocity in the northwestern Alboran Sea. Specifically, upwelling (downwelling) motions tended to increase (decrease) the relative abundance of large phytoplankton, thereby flattening (steepening) the size-abundance spectrum—suggesting that mesoscale motions exert a primary control on the size structure of phytoplankton communities.

Models have been used to address a growing interest in the influence of mesoscale dynamics on the diversity of open-ocean phytoplankton populations, challenging the assumption of environmental homogeneity in Hutchinson's (1961) classic "paradox of the plankton." Using a two-species model with a uniform distribution of limiting resource embedded in quasi-geostrophic turbulence, Bracco et al. (2000) showed how coherent vortices can preserve diversity by isolating populations from the surrounding fluid: A less fit species can persist in conditions in which it would otherwise
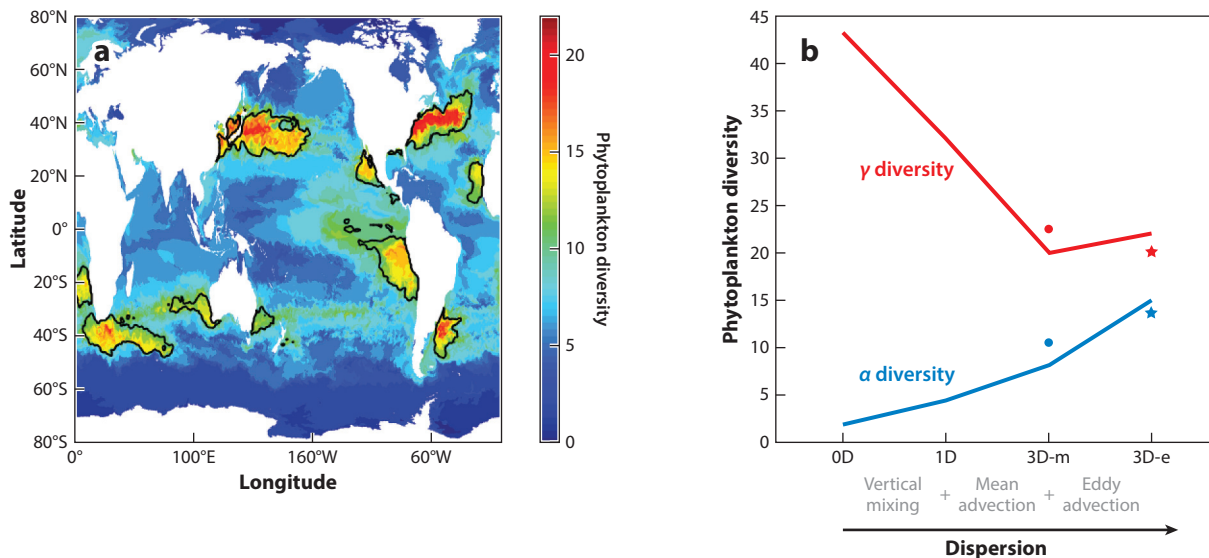
Figure 15

(*a*) Annual average diversity in the surface layer of the high-resolution configuration described by Clayton et al. (2013). Diversity (*α*) is defined as the total number of phytoplankton types with biomass greater than 0.001% of the total phytoplankton biomass. Black contour lines indicate phytoplankton diversity hotspots (*α* > 10.2). (*b*) Trends in local diversity (*α*; 10–100-km scales) and regional diversity (*γ*; 1,000-km scales) as a function of dispersion from the simulations described by Lévy et al. (2014). Experiments 0D, 1D, 3D-m, and 3D-e are ranked along the *x* axis by increasing the level of dispersion in the flow field. In the case with no dispersion (0D), each grid cell in the horizontal and vertical dimensions is treated independently. Vertical mixing is added in the 1D case, and advection by the mean velocity is added in the 3D-m case. The full eddy-resolving flow is accounted for in 3D-e. Results from the latter two experiments are marked with dots and stars, respectively. Panel *a* adapted from Clayton et al. (2013) with permission; panel *b* adapted from Levy et al. (2014) with permission.

be outcompeted if the more fit species were not excluded by the lack of mixing. Perruche et al. (2011) considered a case in which the mesoscale motions influenced the distribution of resources (nutrients), finding that surface quasi-geostrophic turbulence facilitated the coexistence of two competing phytoplankton species. Upwelling in filaments stimulated both species, whereas eddy cores serve as refugia (Bracco et al. 2000).

Additional studies of phytoplankton diversity have been facilitated by the development of the so-called Darwin model, in which many tens of species (ecotypes) are stochastically assigned physiological characteristics with basic allometric trade-offs (Follows et al. 2007). The suite of ecotypes compete in a three-dimensional model ocean, and phytoplankton species composition is an emergent property of the system. Clayton et al. (2013) examined an eddy-permitting case, finding that regions of high eddy kinetic energy in western boundary currents coincide with high diversity in the simulated phytoplankton community (**Figure 15*a***). These diversity hot spots are supported by the confluence of multiple upstream populations, local stimulation via nutrient supply, and environmental variability provided by eddies. Lévy et al. (2014) quantified the impact of dispersal on diversity by applying the Darwin biological module to eddy-resolving simulations in an idealized North Atlantic domain (depicted in **Figure 11*a***). Their counterintuitive results (**Figure 15*b***) suggest that increasing dispersion leads to increasing local diversity (scales on the order of 10–100 km) and decreasing regional diversity (scales on the order of 1,000 km). In other words, hydrodynamic transport leads to the dominance of fewer species overall, but those fewer

species occur over larger ranges with a higher degree of coexistence. Studies of this type are still quite novel, and the data needed to test such models are only beginning to emerge (Clayton et al. 2014, Follows et al. 2007).

7. EFFECTS ON HIGHER TROPHIC LEVELS

Eddy dynamics can perturb oceanic ecosystems, influencing trophic levels ranging from primary producers (as described in Section 6) to top predators. For example, Wiebe & Flierl (1983) described changes in zooplankton (euphausiid) species distributions during the decay of a cold-core ring: native cold-water species such as *Nematoscelis megalops* emigrated, whereas warm-water species such as *Stylocheiron carinatum* immigrated. These changes in distributional patterns were facilitated by vertical positioning behavior in the presence of a hydrodynamic environment that varies with depth. Specifically, the descent of the *N. megalops* population during ring decay resulted in its exit from the region of trapped fluid, thereby bringing about expatriation. By contrast, the near-surface depth-keeping behavior of *S. carinatum* subjects it to enhanced horizontal mixing within the mixed layer, thereby facilitating its invasion into the ring interior. Active vertical positioning also supports a mechanism for concentrating organisms within a mesoscale flow field: depth-keeping behavior in the presence of convergence (Genin et al. 2005, Olson & Backus 1985).

Mesoscale phenomena are also relevant to the transport and survival of planktonic larvae. Lobel & Robinson (1986) noted that a cyclonic eddy near Hawaii retained larval reef fishes for a time period sufficient to complete their pelagic developmental phase and resettle their native reefs. On the other hand, eddies also provide means for enhanced larval dispersal and population connectivity, both in the coastal margin (Mitarai et al. 2009) and in the deep sea (Adams et al. 2011). Bakun (2006) presented a conceptual framework in which eddy-driven variations in productivity offer competing trade-offs in terms of larval survival: Enhanced productivity improves early life nutrition at the expense of increased predator abundance, whereas suppressed productivity decreases the abundance of predators at the expense of poorer larval nutrition. These concepts have been invoked to explain mesoscale variations in the distribution of larval bluefin tuna (Alemany et al. 2010, Lindo-Atichati et al. 2012), sailfish, marlin, swordfish, and other species (Richardson et al. 2010).

Distributions of adult fishes have also been associated with the mesoscale environment. Based on catch data, cyclonic eddies appear to be home to higher abundances of bluefin tuna in the Gulf of Mexico (Teo & Block 2010) and blue marlin in the vicinity of Hawaii (Seki et al. 2002). Acoustic and trawl surveys have shown that midwater fishes are associated with anticyclonic eddies in the Iceland Basin (Godø et al. 2012). Visual sightings of cetaceans (whales and dolphins) in the northern Gulf of Mexico have indicated congregations in or near cyclones and in the confluence of cyclone-anticyclone pairs where zooplankton and micronekton prey abundances were higher (Davis et al. 2002). Seabirds of various kinds have been associated with the peripheries of eddies and convergence zones between them, including great frigate birds in the Mozambique Channel (De Monte et al. 2012, Tew Kai & Marsac 2010, Weimerskirch et al. 2004) and albatross, terns, and shearwaters in the South Indian Ocean (Hyrenbach et al. 2006, Nel et al. 2001). The advent of electronic tagging and telemetry has facilitated investigation of mesoscale niche utilization and behavior by a diverse range of marine animals, including turtles (Gaspar et al. 2006, Kobayashi et al. 2011, Polovina et al. 2004), elephant seals (Bailleul et al. 2010, Campagna et al. 2006, Cotté et al. 2015), shearwaters (Yoda et al. 2014), and penguins (Cotté et al. 2007). In many cases, the association of these animals with mesoscale features is directly linked with foraging behavior.

8. CONCLUDING REMARKS

Advances in theory, observation, and modeling have facilitated substantial progress in understanding of physical-biological-biogeochemical interactions in the ocean. It has become abundantly clear that the impacts of eddies vary regionally (Section 3.7) by virtue of the wealth of processes that contribute (Sections 3.1–3.6) and variations in the relative amplitudes at which those mechanisms are expressed. The long-standing debate about the magnitude of the eddy-induced nutrient source in the subtropics continues (Section 4.1), whereas potential eddy-driven nutrient sinks have become apparent in subpolar gyres (Section 4.2) and in coastal upwelling regions (Section 4.3). Appreciation is growing for the role of mesoscale processes in biological dynamics, including eddy-induced Reynolds stresses (Section 5), planktonic biodiversity (Section 6), and niche utilization by higher trophic levels (Section 7). Future prospects are bright for further progress in these areas as observational capabilities improve in towed instrumentation (Davis et al. 2005), autonomous platforms (Johnson et al. 2009), genomic methods to characterize planktonic communities (DeLong et al. 2006), and electronic tagging technologies (Block et al. 2001). Increased spatial resolution in upcoming altimeter missions (Fu & Ubelmann 2013) and finer spectral resolution in ocean color missions (Del Castillo 2012) will enhance the ability to characterize physical and biological properties in the upper ocean. Likewise, computational infrastructure and modeling capabilities continue to progress (Hecht & Hasumi 2008). This confluence of advances in in situ observation, remote sensing, and modeling has set the stage for further elucidation of the linkages between mesoscale and submesoscale dynamics (Lévy et al. 2012a), which is perhaps one of the most challenging and exciting prospects for future research in this area.

DISCLOSURE STATEMENT

The author is not aware of any affiliations, memberships, funding, or financial holdings that might be perceived as affecting the objectivity of this review.

ACKNOWLEDGMENTS

LITERATURE CITED

Abraham ER. 1998. The generation of plankton patchiness by turbulent stirring. *Nature* 391:577–80

Adams DK, McGillicuddy DJ Jr, Zamudio L, Thurnherr AM, Liang X, et al. 2011. Surface-generated mesoscale eddies transport deep-sea products from hydrothermal vents. *Science* 332:580–83

Alemany F, Quintanilla L, Velez-Belchí P, García A, Cortés D, et al. 2010. Characterization of the spawning habitat of Atlantic bluefin tuna and related species in the Balearic Sea (western Mediterranean). *Prog. Oceanogr.* 86:21–38

Allen JT, Brown L, Sanders R, Moore CM, Mustard A, et al. 2005. Diatom carbon export enhanced by silicate upwelling in the northeast Atlantic. *Nature* 437:728–32

Altabet MA, Ryabenko E, Stramma L, Wallace DWR, Frank M, et al. 2012. An eddy-stimulated hotspot for fixed nitrogen-loss from the Peru oxygen minimum zone. *Biogeosciences* 9:4897–908

Angel MV, Fasham MJR. 1983. Eddies and biological processes. In *Eddies in Marine Science*, ed. AR Robinson, pp. 492–524. Berlin: Springer-Verlag

Bailleul F, Cotté C, Guinet C. 2010. Mesoscale eddies as foraging area of a deep-diving predator, the southern elephant seal. *Mar. Ecol. Prog. Ser.* 408:251–64

Bakun A. 2006. Fronts and eddies as key structures in the habitat of marine fish larvae: opportunity, adaptive response and competitive advantage. *Sci. Mar.* 70S2:105–22

Benitez-Nelson CR, Bidigare RR, Dickey TD, Landry MR, Leonard CL, et al. 2007. Mesoscale eddies drive increased silica export in the subtropical Pacific Ocean. *Science* 316:1017–21

Bibby TS, Moore CM. 2011. Silicate:nitrate ratios of upwelled waters control the phytoplankton community sustained by mesoscale eddies in sub-tropical North Atlantic and Pacific. *Biogeosciences* 8:657–66

Bidigare RR, Benitez-Nelson C, Leonard CL, Quay PD, Parsons ML, et al. 2003. Influence of a cyclonic eddy on microheterotroph biomass and carbon export in the lee of Hawaii. *Geophys. Res. Lett.* 30:1318

Block BA, Dewar H, Blackwell SB, Williams TD, Prince ED, et al. 2001. Migratory movements, depth preferences, and thermal biology of Alantic bluefin tuna. *Science* 293:1310–14

Bourbonnais A, Altabet MA, Charoenpong CN, Larkum J, Hu H, et al. 2015. N-loss isotope effects in the Peru oxygen minimum zone studied using a mesoscale eddy as a natural tracer experiment. *Glob. Biogeochem. Cycles* 29:793–811

Bracco A, Provenzale A, Scheuring I. 2000. Mesoscale vortices and the paradox of the plankton. *Proc. R. Soc. Lond. B* 267:1795–800

Brentnall SJ, Richards KJ, Brindley J, Murphy E. 2003. Plankton patchiness and its effect on larger-scale productivity. *J. Plankton Res.* 25:121–40

Broecker WS, Peng TH. 1982. *Tracers in the Sea*. Palisades, NY: Lamont-Doherty Geol. Obs.

Brzezinski MA, Villareal TA, Lipschultz F. 1998. Silica production and the contribution of diatoms to new and primary production on the central North Pacific. *Mar. Ecol. Prog. Ser.* 167:89–104

Campagna C, Piola AR, Rosa Marin M, Lewis M, Fernández T. 2006. Southern elephant seal trajectories, fronts and eddies in the Brazil/Malvinas Confluence. *Deep-Sea Res. I* 53:1907–24

Charria G, Mélin F, Dadou I, Radenac M-H, Garçon V. 2003. Rossby wave and ocean color: the cells uplifting hypothesis in the South Atlantic Subtropical Convergence Zone. *Geophys. Res. Lett.* 30:1125

Chelton DB, Gaube P, Schlax MG, Early JJ, Samelson RM. 2011a. The influence of nonlinear mesoscale eddies on near-surface oceanic chlorophyll. *Science* 334:328–32

Chelton DB, Schlax MG. 1996. Global observations of oceanic Rossby waves. *Science* 272:234–38

Chelton DB, Schlax MG, Freilich MH, Milliff RF. 2004. Satellite measurements reveal persistent small-scale features in ocean winds. *Science* 303:978–83

Chelton DB, Schlax MG, Samelson RM. 2011b. Global observations of nonlinear mesoscale eddies. *Prog. Oceanogr.* 91:167–216

Chelton DB, Schlax MG, Samelson RM, de Szoeke RA. 2007. Global observations of large oceanic eddies. *Geophys. Res. Lett.* 34:L15606

Cipollini P, Cromwell D, Challenor PG, Raffaglio S. 2001. Rossby waves detected in global ocean colour data. *Geophys. Res. Lett.* 28:323–26

Clayton S, Dutkiewicz S, Jahn O, Follows MJ. 2013. Dispersal, eddies, and the diversity of marine phytoplankton. *Limnol. Oceanogr. Fluids Environ.* 3:182–97

Clayton S, Nagai T, Follows MJ. 2014. Fine scale phytoplankton community structure across the Kuroshio Front. *J. Plankton Res.* 36:1017–30

Cotté C, d'Ovidio F, Dragon AC, Guinet C, Lévy M. 2015. Flexible preference of southern elephant seals for distinct mesoscale features within the Antarctic Circumpolar Current. *Prog. Oceanogr.* 131:46–58

Cotté C, Park Y-H, Guinet C, Bost C-A. 2007. Movements of foraging king penguins through marine mesoscale eddies. *Proc. R. Soc. Lond. B* 274:2385–91

Crawford WR, Brickley PJ, Thomas AC. 2007. Mesoscale eddies dominate surface phytoplankton in northern Gulf of Alaska. *Prog. Oceanogr.* 75:287–303

d'Ovidio F, De Monte S, Alvain S, Danonneau Y, Lévy M. 2010. Fluid dynamical niches of phytoplankton types. *PNAS* 107:18366–70

d'Ovidio F, De Monte S, Della Penna A, Cotté C, Guinet C. 2013. Ecological implications of eddy retention in the open ocean: a Lagrangian approach. *J. Phys. A* 46:254023

Dandonneau Y, Vega A, Loisel H, du Penhoat Y, Menkes C. 2003. Oceanic Rossby waves acting as a "hay rake" for ecosystem floating by-products. *Science* 302:1548–51

Davis CS, Thwaites FT, Gallager SM, Hu Q. 2005. A three-axis fast-tow digital video plankton recorder for rapid surveys of plankton taxa and hydrography. *Limnol. Oceanogr. Methods* 3:59–74

Davis RW, Ortega-Ortiz JG, Ribic CA, Evans WE, Biggs DC, et al. 2002. Cetacean habitat in the northern oceanic Gulf of Mexico. *Deep-Sea Res. I* 49:121–42

De Monte S, Cotte C, d'Ovidio F, Lévy M, Le Corre M, Weimerskirch, H. 2012. Frigatebird behaviour at the ocean–atmosphere interface: integrating animal behaviour with multi-satellite data. *J. R. Soc. Interface* 9:3351–58

Del Castillo C. 2012. *Pre-Aerosol, Clouds, and Ocean Ecosystem* (*PACE*) *mission Science Definition Team report*. Rep., NASA, Washington, DC

DeLong EF, Preston CM, Mincer T, Rich V, Hallam SJ, et al. 2006. Community genomics among stratified microbial assemblages in the ocean's interior. *Science* 311:496–503

Dewar WK. 1986. Mixed layers in Gulf Stream rings. *Dyn. Atmos. Oceans* 10:1–29

Dewar WK, Flierl GR. 1987. Some effects of wind on rings. *J. Phys. Oceanogr.* 17:1653–67

Dufois F, Hardman-Mountford NJ, Greenwood J, Richardson AJ, Feng M, et al. 2014. Impact of eddies on surface chlorophyll in the South Indian Ocean. *J. Geophys. Res. Oceans* 119:8061–77

Ebbesmeyer CC, Lindstrom EJ. 1986. Structure and origin of ^{18}C water observed during the POLYMODE Local Dynamics Experiment. *J. Phys. Oceanogr.* 16:443–53

Eden C, Dietze H. 2009. Effects of mesoscale eddy/wind interactions on biological new production and eddy kinetic energy. *J. Geophys. Res.* 114:C05023

Falkowski PG, Ziemann D, Kolber Z, Bienfang PK. 1991. Role of eddy pumping in enhancing primary production in the ocean. *Nature* 352:55–58

Flierl GR. 1981. Particle motions in large-amplitude wave fields. *Geophys. Astrophys. Fluid Dyn.* 18:39–74

Flierl GR, McGillicuddy DJ Jr. 2002. Mesoscale and submesoscale physical-biological interactions. In *The Sea*, Vol. 12: *Biological-Physical Interactions in the Sea*, ed. AR Robinson, JJ McCarthy, BJ Rothschild, pp. 113–85. New York: Wiley & Sons

Follows MJ, Dutkiewicz S, Grant S, Chisholm SW. 2007. Emergent biogeography of microbial communities in a model ocean. *Science* 315:1843–46

Franks PJS, Wroblewski JS, Flierl GR. 1986. Prediction of phytoplankton growth in response to the frictional decay of a warm-core ring. *J. Geophys. Res.* 91:7603–10

Fu L-L, Ubelmann C. 2013. On the transition from profile altimeter to swath altimeter for observing global ocean surface topography. *J. Atmos. Ocean. Technol.* 31:560–68

Gaspar P, Georges J-Y, Fossette S, Lenoble A, Ferraroli S, Le Maho Y. 2006. Marine animal behaviour: Neglecting ocean currents can lead us up the wrong track. *Proc. R. Soc. Lond. B* 273:2697–702

Gaube P, Chelton DB, Samelson RM, Schlax MG, O'Neill LW. 2015. Satellite observations of mesoscale eddy-induced Ekman pumping. *J. Phys. Oceanogr.* 45:104–32

Gaube P, Chelton DB, Strutton PG, Behrenfeld MJ. 2013. Satellite observations of chlorophyll, phytoplankton biomass and Ekman pumping in nonlinear mesoscale eddies. *J. Geophys. Res.* 118:6349–70

Gaube P, McGillicuddy DJ Jr, Chelton DB, Behrenfeld MJ, Strutton PG. 2014. Regional variations in the influence of mesoscale eddies on near-surface chlorophyll. *J. Geophys. Res. Oceans* 119:8195–220

Genin A, Jaffe JS, Reef R, Richter C, Franks PJS. 2005. Swimming against the flow: a mechanism of zooplankton aggregation. *Science* 308:860–62

Gent PR, Willebrand J, McDougall TJ, McWilliams JC. 1995. Parameterizing eddy-induced tracer transports in ocean circulation models. *J. Phys. Oceanogr.* 25:463–74

Godø OR, Samuelsen A, Macaulay GJ, Patel R, Hjøllo SS, et al. 2012. Mesoscale eddies are oases for higher trophic marine life. *PLOS ONE* 7:e30161

Goldman JC. 1988. Spatial and temporal discontinuities of biological processes in pelagic surface waters. In *Toward a Theory on Biological-Physical Interactions in the World Ocean*, ed. BJ Rothschild, pp. 273–96. Dordrecht, Neth.: D. Reidel

Goldman JC, McGillicuddy DJ Jr. 2003. Impact of large marine diatoms growing at low light on episodic new production. *Limnol. Oceanogr.* 48:1176–82

Goodman L. 2011. Application of the Robinson biodynamical theory to turbulence. *Dyn. Atmos. Oceans* 52:8–19

Goodman L, Robinson AR. 2008. On the theory of advective effects on biological dynamics in the sea. III. The role of turbulence in biological–physical interactions. *Proc. R. Soc. Lond. A* 464:555–72

Gower JFR, Denman KL, Holyer RJ. 1980. Phytoplankton patchiness indicates the fluctuation spectrum of mesoscale oceanic structure. *Nature* 288:157–59

Gruber N, Lachkar Z, Frenzel H, Marchesiello P, Munnich M, et al. 2011. Eddy-induced reduction of biological production in eastern boundary upwelling systems. *Nat. Geosci.* 4:787–92

Hecht MW, Hasumi H, eds. 2008. *Ocean Modeling in an Eddying Regime*. Geophys. Monogr. Ser. 177. Washington, DC: Am. Geophys. Union

Hernández-Carrasco I, Rossi V, Hernández-García E, Garçon V, López C. 2014. The reduction of plankton biomass induced by mesoscale stirring: a modeling study in the Benguela upwelling. *Deep-Sea Res. I* 83:65–80

Hutchinson GE. 1961. The paradox of the plankton. *Am. Nat.* 95:137–45

Hyrenbach KD, Veit RR, Weimerskirch H, Hunt GL Jr. 2006. Seabird associations with mesoscale eddies: the subtropical Indian Ocean. *Mar. Ecol. Prog. Ser.* 324:271–79

Jenkins WJ. 1988a. Nitrate flux into the euphotic zone near Bermuda. *Nature* 331:521–23

Jenkins WJ. 1988b. The use of anthropogenic tritium and helium-3 to study subtropical gyre ventilation and circulation. *Philos. Trans. R. Soc.* 325:43–61

Jenkins WJ, Goldman J. 1985. Seasonal oxygen cycling and primary production in the Sargasso Sea. *J. Mar. Res.* 43:465–91

Johnson KS, Berelson WM, Boss ES, Chase Z, Claustre H, et al. 2009. Observing biogeochemical cycles at global scales with profiling floats and gliders: prospects for a global array. *Oceanography* 22(3):216–25

José YS, Aumont O, Machu E, Penven P, Moloney CL, Maury O. 2014. Influence of mesoscale eddies on biological production in the Mozambique Channel: several contrasted examples from a coupled ocean-biogeochemistry model. *Deep-Sea Res. II* 100:79–93

Kahru M, Mitchell BG, Gille ST, Hewes CD, Holm-Hansen O. 2007. Eddies enhance biological production in the Weddell-Scotia Confluence of the Southern Ocean. *Geophys. Res. Lett.* 34:L14603

Killworth PD, Cipollini P, Uz BM, Blundell JR. 2004. Physical and biological mechanisms for planetary waves observed in satellite-derived chlorophyll. *J. Geophys. Res.* 109:C07002

Klein P, Hua BL. 1988. Mesoscale heterogeneity of the wind-driven mixed layer: influence of a quasi-geostrophic flow. *J. Mar. Res.* 46:495–525

Klein P, Lapeyre G. 2009. The oceanic vertical pump induced by mesoscale and submesoscale turbulence. *Annu. Rev. Mar. Sci.* 1:351–75

Knauss JA. 1978. *Introduction to Physical Oceanography*. Englewood Cliffs, NJ: Prentice Hall

Kobayashi DR, Cheng I-J, Parker DM, Polovina JJ, Kamezaki N, Balazs GH. 2011. Loggerhead turtle (*Caretta caretta*) movement off the coast of Taiwan: characterization of a hotspot in the East China Sea and investigation of mesoscale eddies. *ICES J. Mar. Sci.* 68:707–18

Kouketsu S, Tomita H, Oka E, Hosoda S, Kobayashi T, Sato K. 2012. The role of meso-scale eddies in mixed layer deepening and mode water formation in the western North Pacific. *J. Oceanogr.* 68:63–77

Krause JW, Lomas MW, Nelson DM. 2009. Biogenic silica at the Bermuda Atlantic Time-series Study site in the Sargasso Sea: temporal changes and their inferred controls based on a 15-year record. *Glob. Biogeochem. Cycles* 23:GB3004

Krause JW, Nelson DM, Lomas MW. 2010. Production, dissolution, accumulation, and potential export of biogenic silica in a Sargasso Sea mode-water eddy. *Limnol. Oceanogr.* 55:569–79

Kunze E. 1985. Near-inertial wave propagation in geostrophic shear. *J. Phys. Oceanogr.* 15:544–656

Lapeyre G, Klein P. 2006. Impact of the small-scale elongated filaments on the oceanic vertical pump. *J. Mar. Res.* 64:835–51

Lathuilière C, Echevin V, Lévy M, Madec G. 2010. On the role of the mesoscale circulation on an idealized coastal upwelling ecosystem. *J. Geophys. Res.* 115:C09018

Lathuilière C, Lévy M, Echevin V. 2011. Impact of eddy-driven vertical fluxes on phytoplankton abundance in the euphotic layer. *J. Plankton Res.* 33:827–31

Lee MM, Williams RG. 2000. The role of eddies in the isopycnic transfer of nutrients and their impact on biological production. *J. Mar. Res.* 58:895–917

Legendre L, Demers S. 1984. Towards dynamic biological oceanography and limnology. *Can. J. Fish. Aquat. Sci.* 41:2–19

Lehahn Y, d'Ovidio F, Lévy M, Amitai Y, Heifetz E. 2011. Long range transport of a quasi isolated chlorophyll patch by an Agulhas ring. *Geophys. Res. Lett.* 38:L16610

Lehahn Y, d'Ovidio F, Lévy M, Heifetz E. 2007. Stirring of the northeast Atlantic spring bloom: a Lagrangian analysis based on multisatellite data. *J. Geophys. Res.* 112:C08005

Letelier RM, Karl DM, Abbott MR, Flament PJ, Freilich MH, Lukas R. 2000. Role of late winter mesoscale events in the biogeochemical variability of the upper water column of the North Pacific Subtropical Gyre. *J. Geophys. Res.* 105:28723–39

Lévy M. 2008. The modulation of biological production by oceanic mesoscale turbulence. In *Transport and Mixing in Geophysical Flows*, ed. J Weiss, A Provenzale, pp. 219–61. Berlin: Springer

Lévy M, Ferrari R, Franks PJS, Martin AP, Rivière P. 2012a. Bringing physics to life at the submesoscale. *Geophys. Res. Lett.* 39:L14602

Lévy M, Iovino D, Resplandy L, Klein P, Madec G, et al. 2012b. Large-scale impacts of submesoscale dynamics on phytoplankton: local and remote effects. *Ocean Model.* 43–44:77–93

Lévy M, Jahn O, Dutkiewicz S, Follows MJ. 2014. Phytoplankton diversity and community structure affected by oceanic dispersal and mesoscale turbulence. *Limnol. Oceanogr. Fluids Environ.* 4:67–84

Lévy M, Klein P. 2004. Does the low frequency variability of mesoscale dynamics explain a part of the phytoplankton and zooplankton spectral variability? *Proc. R. Soc. Lond. A* 460:1673–87

Lévy M, Klein P, Treguier A-M. 2001. Impact of sub-mesoscale physics on production and subduction of phytoplankton in an oligotrophic regime. *J. Mar. Res.* 59:535–65

Lévy M, Martin AP. 2013. The influence of mesoscale and submesoscale heterogeneity on ocean biogeochemical reactions. *Glob. Biogeochem. Cycles* 27:1139–50

Lévy M, Mémery L, Madec G. 1998. The onset of a bloom after deep winter convection in the northwestern Mediterranean sea: mesoscale process study with a primitive equation model. *J. Mar. Syst.* 16:7–21

Lévy M, Mémery L, Madec G. 1999. The onset of the Spring Bloom in the MEDOC area: mesoscale spatial variability. *Deep-Sea Res. I* 46:1137–60

Lewis MR. 2002. Variability of plankton and plankton processes on the mesoscale. In *Phytoplankton Productivity: Carbon Assimilation in Marine and Freshwater Ecosystems*, ed. PJLB Williams, DN Thomas, CS Reynolds, pp. 141–55. Oxford, UK: Blackwell Sci.

Li J, Qi Y, Jing Z, Wang J. 2014. Enhancement of eddy-Ekman pumping inside anticyclonic eddies with wind-parallel extension: satellite observations and numerical studies in the South China Sea. *J. Mar. Syst.* 132:150–61

Lima ID, Olson DB, Doney SC. 2002. Biological response to frontal dynamics and mesoscale variability in oligotrophic environments: biological production and community structure. *J. Geophys. Res. Oceans* 107:25-1–21

Lindo-Atichati D, Bringas F, Goni G, Muhling B, Muller-Karger FE, Habtes S. 2012. Varying mesoscale structures influence larval fish distribution in the northern Gulf of Mexico. *Mar. Ecol. Prog. Ser.* 463:245–57

Lobel PS, Robinson AR. 1986. Transport and entrapment of fish larvae by ocean mesoscale eddies and currents in Hawaiian waters. *Deep-Sea Res. A* 33:483–500

Mackas DL, Denman KL, Abbott MR. 1985. Plankton patchiness: biology in the physical vernacular. *Bull. Mar. Sci.* 37:652–74

Mahadevan A. 2016. The impact of submesoscale physics on primary productivity of plankton. *Annu. Rev. Mar. Sci.* 8:161–84

Mahadevan A, D'Asaro E, Lee C, Perry MJ. 2012. Eddy-driven stratification initiates North Atlantic spring phytoplankton blooms. *Science* 337:54–58

Mahadevan A, Thomas LN, Tandon A. 2008. Comment on "Eddy/wind interactions stimulate extraordinary mid-ocean plankton blooms." *Science* 320:448

Marshall D. 1997. Subduction of water masses in an eddying ocean. *J. Mar. Res.* 55:201–22

Martin AP. 2003. Phytoplankton patchiness: the role of lateral stirring and mixing. *Prog. Oceanogr.* 57:125–74

Martin AP, Lévy M, van Gennip S, Pardo S, Srokosz M, et al. 2015. An observational assessment of the influence of mesoscale and submesoscale heterogeneity on ocean biogeochemical reactions. *Glob. Biogeochem. Cycles* 29:1421–38

Martin AP, Pondaven P. 2003. On estimates for the vertical nitrate flux due to eddy pumping. *J. Geophys. Res. Oceans* 108:3359

Martin AP, Richards KJ. 2001. Mechanisms for vertical nutrient transport within a North Atlantic mesoscale eddy. *Deep-Sea Res. II* 48:757–73

Martin AP, Richards KJ, Law CS, Liddicoat M. 2001. Horizontal dispersion within an anticyclonic mesoscale eddy. *Deep-Sea Res. II* 48:739–55

McGillicuddy DJ Jr. 2011. Eddies masquerade as planetary waves. *Science* 334:318–19

McGillicuddy DJ Jr. 2015. Formation of intra-thermocline lenses by eddy-wind interaction. *J. Phys. Oceanogr.* 45:606–12

McGillicuddy DJ Jr, Anderson LA, Bates NR, Bibby T, Buesseler KO, et al. 2007. Eddy/wind interactions stimulate extraordinary mid-ocean plankton blooms. *Science* 316:1021–26

McGillicuddy DJ Jr, Anderson LA, Doney SC, Maltrud ME. 2003. Eddy-driven sources and sinks of nutrients in the upper ocean: results from a 0.1° resolution model of the North Atlantic. *Glob. Biogeochem. Cycles* 17:1035

McGillicuddy DJ Jr, Robinson AR. 1997. Eddy induced nutrient supply and new production in the Sargasso Sea. *Deep-Sea Res. I* 44:1427–49

McGillicuddy DJ Jr, Robinson AR, McCarthy JJ. 1995. Coupled physical and biological modeling of the spring bloom in the North Atlantic (II): three dimensional bloom and post-bloom effects. *Deep-Sea Res. I* 42:1359–98

McGillicuddy DJ Jr, Robinson AR, Siegel DA, Jannasch HW, Johnson R, et al. 1998. Influence of mesoscale eddies on new production in the Sargasso Sea. *Nature* 394:263–65

McNeil JD, Jannasch HW, Dickey TD, McGillicuddy DJ Jr, Brzezinski M, Sakamoto CM. 1999. New chemical, bio-optical and physical observations of upper ocean response to the passage of a mesoscale eddy off Bermuda. *J. Geophys. Res.* 104:15537–48

McWilliams JC. 2008. The nature and consequences of oceanic eddies. See Hecht & Hasumi 2008, pp. 5–15

Menkes CE, Kennan SC, Flament P, Dandonneau Y, Masson S, et al. 2002. A whirling ecosystem in the equatorial Atlantic. *Geophys. Res. Lett.* 29:48-1–4

Mitarai S, Siegel DA, Watson JR, Dong C, McWilliams JC. 2009. Quantifying connectivity in the coastal ocean with application to the Southern California Bight. *J. Geophys. Res. Oceans* 114:C10026

Mizobata K, Saitoh SI, Shiomoto A, Miyamura T, Shiga N, et al. 2002. Bering Sea cyclonic and anticyclonic eddies observed during summer 2000 and 2001. *Prog. Oceanogr.* 55:65–75

Moore TS, Matear RJ, Marra J, Clementson L. 2007. Phytoplankton variability off the Western Australian Coast: mesoscale eddies and their role in cross-shelf exchange. *Deep-Sea Res. II* 54:943–60

Nel DC, Lutjeharms JRE, Pakhomov EA, Ansorge IJ, Ryan PG, Klages NTW. 2001. Exploitation of mesoscale oceanographic features by grey-headed albatross *Thalassarche chrysostoma* in the southern Indian Ocean. *Mar. Ecol. Prog. Ser.* 217:15–26

Nelson DM, McCarthy JJ, Joyce TM, Ducklow HW. 1989. Enhanced near-surface nutrient availability and new production resulting from the frictional decay of a Gulf Stream warm-core ring. *Deep-Sea Res. A* 36:705–14

Niiler PP. 1969. On the Ekman divergence in an oceanic jet. *J. Geophys. Res.* 74:7048–52

NOAA (Natl. Ocean. Atmos. Admin.). 2009. *World Ocean Atlas 2009.* **https://www.nodc.noaa.gov/OC5/WOA09/pr_woa09.html**

Nurser AJG, Zhang JW. 2000. Eddy-induced mixed layer shallowing and mixed layer/thermocline exchange. *J. Geophys. Res. Oceans* 105:21851–68

Olaizola M, Ziemann DA, Bienfang PK, Walsh WA, Conquest LD. 1993. Eddy-induced oscillations of the pycnocline affect the floristic composition and depth distribution of phytoplankton in the subtropical Pacific. *Mar. Biol.* 116:533–42

Olson DB, Backus RH. 1985. The concentrating of organisms at fronts: a cold-water fish and a warm-core Gulf Stream ring. *J. Mar. Res.* 43:113–37

Oschlies A. 2002. Can eddies make ocean deserts bloom? *Glob. Biogeochem. Cycles* 16:1106

Oschlies A. 2008. Eddies and upper-ocean nutrient supply. See Hecht & Hasumi 2008, pp. 115–30

Oschlies A, Garçon V. 1998. Eddy-induced enhancement of primary production in a model of the North Atlantic Ocean. *Nature* 394:266–69

Pascual A, Faugère Y, Larnicol G, LeTraon PY. 2006. Improved description of the ocean mesoscale variability by combining four satellite altimeters. *Geophys. Res. Lett.* 33:L02611

Pasquero C, Bracco A, Provenzale A. 2005. Impact of the spatiotemporal variability of the nutrient flux on primary productivity in the ocean. *J. Geophys. Res. Oceans* 110:C07005

Pearce AF, Griffiths RW. 1991. The mesoscale structure of the Leeuwin Current: a comparison of laboratory models and satellite imagery. *J. Geophys. Res. Oceans* 96:16739–57

Perruche C, Rivière P, Lapeyre G, Carton X, Pondaven P. 2011. Effects of surface quasi-geostrophic turbulence on phytoplankton competition and coexistence. *J. Mar. Res.* 69:105–35

Pingree RD, Holligan PM, Mardell GT. 1979. Phytoplankton growth and cyclonic eddies. *Nature* 278:245–47

Polovina JJ, Balazs GH, Howell EA, Parker DM, Seki MP, Dutton PH. 2004. Forage and migration habitat of loggerhead (*Caretta caretta*) and olive ridley (*Lepidochelys olivacea*) sea turtles in the central North Pacific Ocean. *Fish. Oceanogr.* 13:36–51

Prasanna Kumar S, Nuncio M, Ramaiah N, Sardesai S, Narvekar J, et al. 2007. Eddy-mediated biological productivity in the Bay of Bengal during fall and spring intermonsoons. *Deep-Sea Res. I* 54:1619–40

Provenzale A. 1999. Transport by coherent barotropic vortices. *Annu. Rev. Fluid Mech.* 31:55–93

Radchenko LA. 1983. Quantitative distribution of seston in the region. In *Experimental Investigations Under the International POLYMODE Program*, ed. BA Nelepo, pp. 129–35. New Delhi, India: Oxonian

Resplandy L, Lévy M, Madec G, Pous S, Aumont O, Kumar D. 2011. Contribution of mesoscale processes to nutrient budgets in the Arabian Sea. *J. Geophys. Res. Oceans* 116:C11007

Richardson DE, Llopiz JK, Guigand CM, Cowen RK. 2010. Larval assemblages of large and medium-sized pelagic species in the Straits of Florida. *Prog. Oceanogr.* 86:8–20

Ring Group. 1981. Gulf Stream cold-core rings: their physics, chemistry and biology. *Science* 212:1091–100

Rodriguez J, Tintore J, Allen JT, Blanco JM, Gomis D, et al. 2001. Mesoscale vertical motion and the size structure of phytoplankton in the ocean. *Nature* 410:360–63

Rossi V, López C, Sudre J, Hernández-García E, Garçon V. 2008. Comparative study of mixing and biological activity of the Benguela and Canary upwelling systems. *Geophys. Res. Lett.* 35:L11602

Roukhiyainen MI, Yunev OA. 1983. Phytoplankton and primary productin in the wester Sargasso Sea in summer 1977. In *Experimental Investigations Under the International POLYMODE Program*, ed. BA Nelepo, pp. 120–28. New Delhi, India: Oxonian

Seki MP, Lumpkin R, Flament P. 2002. Hawaii cyclonic eddies and blue marlin catches: the case study of the 1995 Hawaiian International Billfish Tournament. *J. Oceanogr.* 58:739–45

Seki MP, Polovina JJ, Brainard RE, Bidigare RR, Leonard CL, Foley DG. 2001. Biological enhancement at cyclonic eddies tracked with GOES thermal imagery in Hawaiian waters. *Geophys. Res. Lett.* 28:1583–86

Shulenberger E, Reid JL. 1981. The Pacific shallow oxygen maximum, deep chlorophyll maximum, and primary productivity, reconsidered. *Deep-Sea Res. A* 28:901–19

Siegel DA, Court DB, Menzies DW, Peterson P, Maritorena S, Nelson NB. 2008. Satellite and in situ observations of the bio-optical signatures of two mesoscale eddies in the Sargasso Sea. *Deep-Sea Res. II* 55:1218–30

Siegel DA, Peterson P, McGillicuddy DJ Jr, Maritorena S, Nelson NB. 2011. Bio-optical footprints created by mesoscale eddies in the Sargasso Sea. *Geophys. Res. Lett.* 38:L13608

Srokosz MA, Martin AP, Fasham MJR. 2003. On the role of biological dynamics in plankton patchiness at the mesoscale: an example from the eastern North Atlantic Ocean. *J. Mar. Res.* 61:517–37

Stern ME. 1965. Interaction of a uniform wind stress with a geostrophic vortex. *Deep-Sea Res. Oceanogr. Abstr.* 12:355–67

Stramma L, Bange HW, Czeschel R, Lorenzo A, Frank M. 2013. On the role of mesoscale eddies for the biological productivity and biogeochemistry in the eastern tropical Pacific Ocean off Peru. *Biogeosciences* 10:7293–306

Strass VH. 1992. Chlorophyll patchiness caused by mesoscale upwelling at fronts. *Deep-Sea Res. A* 39:75–96

Sweeney EN, McGillicuddy DJ Jr, Buesseler KO. 2003. Biogeochemical impacts due to mesoscale eddy activity in the Sargasso Sea as measured at the Bermuda Atlantic Time-series (BATS) site. *Deep-Sea Res. II* 50:3017–39

Teo SLH, Block BA. 2010. Comparative influence of ocean conditions on yellowfin and Atlantic bluefin tuna catch from longlines in the Gulf of Mexico. *PLOS ONE* 5:e10756

Tew Kai E, Marsac F. 2010. Influence of mesoscale eddies on spatial structuring of top predators' communities in the Mozambique Channel. *Prog. Oceanogr.* 86:214–23

Uz BM, Yoder JA, Osychny V. 2001. Pumping of nutrients to ocean surface waters by the action of propagating planetary waves. *Nature* 409:597–600

Vaillancourt RD, Marra J, Seki MP, Parsons ML, Bidigare RR. 2003. Impact of a cyclonic eddy on phytoplankton community structure and photosynthetic competency in the subtropical North Pacific Ocean. *Deep-Sea Res. I* 50:829–47

Venrick EL. 1990. Mesoscale patterns of chlorophyll *a* in the central North Pacific. *Deep-Sea Res. A* 37:1017–31

Waite AM, Thompson PA, Pesant S, Feng M, Beckley LE, et al. 2007. The Leeuwin Current and its eddies: an introductory overview. *Deep-Sea Res. II* 54:789–96

Wallhead PJ, Garçon VC, Martin AP. 2013. Efficient upscaling of ocean biogeochemistry. *Ocean Model.* 63:40–55

Wallhead PJ, Martin AP, Srokosz MA. 2008. Spatially implicit plankton population models: transient spatial variability. *J. Theor. Biol.* 253:405–23

Warm Core Rings Exec. Comm. 1982. Multidisciplinary program to study warm core rings. *Eos Trans. AGU* 63:834–35

Weimerskirch H, Corre ML, Jaquemet S, Potier M, Marsac F. 2004. Foraging strategy of a top predator in tropical waters: great frigatebirds in the Mozambique Channel. *Mar. Ecol. Prog. Ser.* 275:297–308

Wiebe PH, Flierl GR. 1983. Euphausiid invasion/dispersal in Gulf Stream cold-core rings. *Aust. J. Mar. Freshw. Res.* 34:625–52

Wiebe PH, Joyce TM. 1992. Introduction to interdisciplinary studies of Kuroshio and Gulf Stream rings. *Deep-Sea Res. A* 39(Suppl. 1):v–vi

Williams RG. 1988. Modification of ocean eddies by air-sea interaction. *J. Geophys. Res. Oceans* 93:15523–33

Williams RG, Follows MJ. 1998. The Ekman transfer of nutrients and maintenance of new production over the North Atlantic. *Deep-Sea Res. I* 45:461–89

Williams RG, Follows MJ. 2003. Physical transport of nutrients and the maintenance of biological production. In *Ocean Biogeochemistry: The Role of the Ocean Carbon Cycle in Global Change*, ed. MJR Fasham, pp. 19–51. Berlin: Springer-Verlag

Williams RG, Follows MJ. 2011. *Ocean Dynamics and the Carbon Cycle: Principles and Mechanisms*. Cambridge, UK: Cambridge Univ. Press

Woods JD. 1988. Mesoscale upwelling and primary production. In *Toward a Theory on Biological-Physical Interactions in the World Ocean*, ed. BJ Rothschild, pp. 7–23. Dordrecht, Neth.: D. Reidel

Xiu P, Chai F. 2011. Modeled biogeochemical responses to mesoscale eddies in the South China Sea. *J. Geophys. Res. Oceans* 116:C10006

Xiu P, Palacz AP, Chai F, Roy EG, Wells ML. 2011. Iron flux induced by Haida eddies in the Gulf of Alaska. *Geophys. Res. Lett.* 38:L13607

Yoda K, Shiomi K, Sato K. 2014. Foraging spots of streaked shearwaters in relation to ocean surface currents as identified using their drift movements. *Prog. Oceanogr.* 122:54–64

Yoshimori A, Kishi MJ. 1994. Effects of interaction between two warm-core rings on phytoplankton distribution. *Deep-Sea Res. I* 41:1039–52

Zhou K, Dai M, Kao S-J, Wang L, Xiu P, et al. 2013. Apparent enhancement of [234]Th-based particle export associated with anticyclonic eddies. *Earth Planet. Sci. Lett.* 381:198–209

Contents

Errata

An online log of corrections to *Annual Review of Marine Science* articles may be found at
http://www.annualreviews.org/errata/marine